NTNU – Trondheim
Norwegian University of
Science and Technology

Oxidation of Liquid Silicon in a Medium Scale Induction Furnace

Examination of the Fuming Rate and Fume Composition

Nicholas Smith

Silicon and Ferroalloy Production
Submission date: June 2012
Supervisor: Gabriella Tranell, IMTE

Norwegian University of Science and Technology
Department of Materials Science and Engineering

Abstract

The aim of this work was to study the effect of flow rate on the fuming rate/silica flux of liquid silicon in order to gain a better understanding of the silica fuming during industrial ladle refining during silicon production. The formation of silica fume is the results when the liquid silicon is exposed to air. This silica fume has been shown to be a health hazard when breathed by plant workers and increased environmental regulations call for its elimination. This work is being done as part of the FUME project (FUgitive emissions of Materials and Energy) with funding from the Norwegian Research Council and the Ferro-alloys Industrial Research Association (FFF).

To examine the silica flux a series of experiments in a medium scale induction furnace were carried out. A graphite crucible with an inside diameter of 11.4 cm was charged with refined or unrefined metallurgical grade silicon. This silicon was melted and air was blown onto the surface at 3 different rates (1, 3.5, 5 LPM). The produced silica fume was collected in a filter and analyzed for particle size and compositions differences. The total mass of the fume produced was used to estimate the silica flux.

The silica flux was found to vary with flow rate from 0.00156 moles/s-m^2 at 1 LPM to 0.02788 moles/s-m^2 at 5 LPM. With no significant difference between refined and unrefined. The particle size and composition were also found to vary with flow rate. The particle size distribution was similar to what was found in industry (75% under 0.01 µm). However, the size of the largest particles was found to decrease with increasing flow rate. Finally the amount of impurities in the fume decreased with increasing flow rate as well.

Additionally, in continuation of previous work on small scale oxidation experiments with liquid silicon in a muffle furnace were done and a more in-depth analysis by EPMA was carried out. It was found that addition of calcium increases the oxidation rate, and that the addition of calcium and aluminum results in an oxide layer with multiple phases.

Acknowledgement

I would like to thank my advisor Gabriella Tranell for her help and advice with the experimental work and analysis carried out in this thesis. Additionally, I would like to thank the other members of the Fume Project Mari Næss and Ida Kero for their advice and help with the experiments and writing. Finally, I would like to thank Delphine Leroy for her assistance in setting up and running the experiments.

Table of Contents

List of Figures

List of Tables

1 Introduction

During the production of metallurgical grade silicon the liquid metal is exposed to air during tapping and refining. Upon exposure of the silicon to oxygen it will oxidize to form a silica fume. When compared to the total amount of silicon metal the amount lost to fume in minor, however the silica fume does pose a health and environmental risk. Especially to those working in the plants. To date little study has been made to study the amounts and composition of the fume. During refining of the silicon the metal is exposed to air while in being transported in uncovered ladles and during purging. This air causes the oxidation of the silicon to form a fume which the workers can then potentially breathe. To better understand this fuming a series of medium scale experiments in an induction furnace will be carried out. In addition to a continuation of the small scale experiments carried out in a muffle furnace.

The goal of this work is to study the flux of the silica fume in a medium scale induction furnace. One of the key steps in the production of metallurgical grade silicon (MG-silicon) is the refining to remove calcium and aluminum. This is accomplished by purging air from the bottom of the ladle through the silicon melt this oxidizes the impurity elements into a slag phase. Previous work has shown that oxidation at the surface is the source of the majority of the fume. Therefore, in these experiments air will be blown over the surface of liquid silicon and the produced fume will be captured in a filter and analyzed.

In a medium scale induction furnace (75 kW) both refined and unrefined MG-silicon will be melted and then oxidized by blowing air onto the surface. Three different airflows will be tested 1, 3.5 and 5 LPM. The silica fume that forms will be measured and analyzed. To determine the silica flux a mass balance will be carried out; the silica fume will be captured in a filter. The mass gain of this silica fume will then used to calculate the silica flux in moles/s-m^2. Additionally, samples of the fume will be analyzed with SEM and EDS for size and composition differences.

In continuation of work previously carried out a series of oxidation experiments in a muffle furnace under still air will be undertaken. In addition to further analysis of the

samples from previous experiments in the muffle furnace. The goal of the experiments is to determine the effects of calcium and aluminum on the oxidation rate of liquid silicon. Previously, samples containing 1% Al, 0.5% Ca or 1% Al-0.5% Ca were oxidized at 1550℃ and 1600℃ and the oxidation rate calculated from the mass gain. In this work the 0.5% Ca samples will be rerun in an attempt to remove some discrepancies in the original results, and all the samples will be examined in the electron microprobe (EPMA).

This work is being done under the FUME project (FUgitive emissions of Materials and Energy) a project funded by the Norwegian Research Council and the Ferro-alloys Industrial Research Association (FFF). The goal of the project is to study and model all emissions related to the production of ferroalloys of both material and energy.

2 Theory

2.1 Oxidation of Liquid Silicon

The oxidation of liquid silicon has seen limited study. However, oxidation of solid silicon at elevated temperatures has been studied by several researchers over the past 60 years. This previous work will form the basis of the theory for the oxidation of liquid silicon. The most prominent work on solid silicon was done by Wagner in 1958 and Turkdogan et al. in 1963. [(1) (2)] Wagner's model was developed specifically for silicon, whereas, Turkdogan's model was developed as a general theory of oxidation for all metals at elevated temperature. Both models have been used and modified over the past 60 years and there is still no widely excepted single model for the oxidation of solid silicon. The general mechanisms for oxidation are given below followed by a more in depth examination of the Wagner and Turkdogan models.

It is generally assumed that there are four possible reactions when silicon and oxygen interact. These are given as equations 1-4 below. Which reaction happen depends on the partial pressure of oxygen, partial pressure of SiO and the temperature.

$$Si_{(s,l)} + \tfrac{1}{2}O_{2(g)} = SiO_{(g)} \qquad \text{Equation 1}$$

$$Si_{(s,l)} + O_{2(g)} = SiO_{2(g,s)} \qquad \text{Equation 2}$$

$$\tfrac{1}{2}Si_{(s,l)} + \tfrac{1}{2}SiO_{2\,(g,s)} = SiO_{(g)} \qquad \text{Equation 3}$$

$$SiO_{(g)} + \tfrac{1}{2}O_{2(g)} = SiO_{2(g,s)} \qquad \text{Equation 4}$$

One of the major factors effecting oxidation rate is whether it is active or passive oxidation. Active oxidation occurs when the oxygen partial pressure is low; as a result reaction 1 occurs and SiO gas forms above the silicon surface. Passive oxidation occurs when the oxidation product is solid SiO_2 which forms directly on the surface through reaction 2 or a combination of reactions 1 and 4. Since the reaction between silicon and oxygen is nearly instantaneous it is generally assumed that the oxidation is mass transfer controlled and it is the supply of oxygen to the surface that is the rate

limiting step. Due to this passive oxidation has a significantly lower oxidation rate than active oxidation, because the diffusion of oxygen through solid SiO_2 is much slower than diffusion through a gas boundary layer.

Table 1 shows the variables that are considered to have a major impact on the oxidation rate of liquid silicon and the effect they have on the system. In the temperature range of concern the effect of temperature is limited because the increase in diffusion rate is offset by the change in reaction rate.

Table 1 Main factors affecting the oxidation rate of solid silicon.

Variable	Effect on oxidation rate
Gas composition	P_{SiO}, P_{O2}, diffusion through inert gasses
Gas Flow Rate	Surface turbulence, boundary layer thickness, gas diffusion
Temperature	P_{SiO}, diffusion coefficients

Regardless of the model used it is widely accepted that in still air with a P_{O2} of 0.21 atm the silicon will be in the passive oxidation regime. To remain in the active oxidation regime conditions must exist were the SiO_2 layer is lost at the same rate which it forms.

2.1.1 Wagner Model

The first theory on the oxidation of silicon was proposed by Wagner in 1958. [(1)] Where he studied and modeled the active-passive transition on silicon. The model was based on equations 1 and 4 where equation 1 is the silicon oxidation reaction. If the partial pressure of SiO is below a critical value the surface would be free of solid SiO_2. However, if the SiO pressure is above the critical pressure then solid silica will exist.

The starting point for this model is a surface free from silica and an oxygen partial pressure of zero. As the pressure of oxygen is increased the resulting SiO pressure is increased according to equation 1. The SiO pressure will increase until it reaches the critical value need for silica formation given by equation 4. A schematic of the model is given in Figure 1 below.

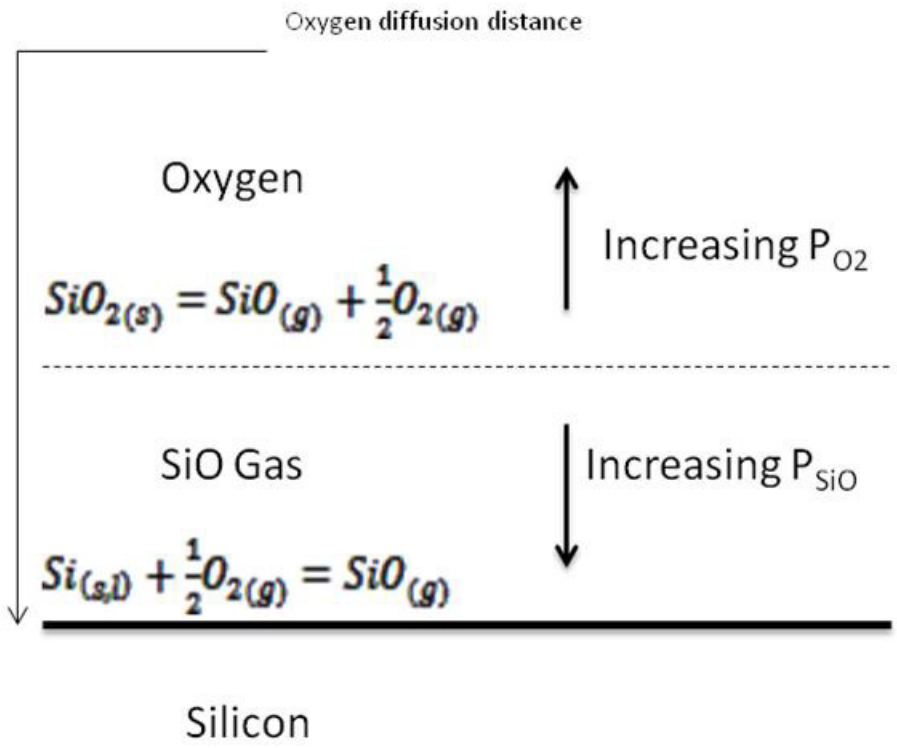

Figure 1--Schematic of the oxidation mechanism proposed by Wagner.

To derive the flux of silicon from the surface Wagner assumed that the reaction between oxygen and silicon is instantaneous, and rate limiting step is the transport of oxygen to the melt surface and SiO away from the surface. This is can be confirmed by looking at the low activation energies for equations 1-4. Under steady state conditions it is said that the oxygen flowing into the surface must equal the flow of oxygen out as SiO. This can be written as equations 5 and further developed to equation 6.

$$j_{O_2 in} = j_{SiO\ out} \qquad \text{Equation 5}$$

$$\frac{2D_{O_2}p^{\circ}_{O_2}}{\delta_{O_2}RT} = \frac{D_{SiO}p^{*}_{SiO}}{\delta_{SiO}RT} \qquad \text{Equation 6}$$

Here *D* is the diffusivity of the specified gas species, $p^{\circ}_{O_2}$ is the partial pressure of oxygen in the bulk, p^{*}_{SiO} is the partial pressure of SiO at the surface and δ is the boundary layer thickness. Equation 6 can be rearranged to give the SiO pressure as shown in equation 7,

$$p^*_{SiO} = 2p^{\circ}_{O_2} \frac{D_{O_2}}{D_{SiO}} \frac{\delta_{SiO}}{\delta_{O_2}}$$ Equation 7

and if equation 8 is assumed.

$$\frac{\delta_{SiO}}{\delta_{O_2}} = \frac{D_{SiO}}{D_{O_2}}^{0.5}$$ Equation 8

Then it can be said that the maximum oxygen partial pressure that a bare surface can be maintained is given by equation 9.

$$p^{\circ}_{O_2}(max) \cong \frac{1}{2}(\frac{D_{SiO}}{D_{O_2}})^{0.5} \mathrm{p_{SiO(eq)}}$$ Equation 9

Wagner found this to be a value of 6.1×10^{-3} atm at 1410°C. At oxygen pressures above this the surface will be covered by a layer of solid silica and the oxidation rate will be nearly zero.

Once a layer of silica is formed on the surface the steady state layer thickness will be obtained when the rate of diffusion across the layer equals the rate of consumption by equation 3. The transport of oxygen to the surface is then defined by equation 10.

$$j'_o = \frac{2D_{O_2}(p^{\circ}_{O_2} - p^*_{O_2})}{\delta_{O_2} RT}$$ Equation 10

The rate of loss of silicon is given by equation 11; which was formed by inserting equations 6, 8 and 10 into equation 5.

$$j_{Si} = \frac{D_{SiO} P^*_{SiO}}{\delta_{SiO} RT} = \frac{D_{SiO} K}{(P^{\circ}_{O_2})^{0.5} \delta_{SiO} RT}$$ Equation 11

Where *K* is the equilibrium constant defined by equation 12.

$$p^*_{SiO}(p^*_{O_2})^{0.5} = K$$ Equation 12

Figure 2 shows a plot developed by Wagner of silicon flux versus oxygen pressure. It can be seen that at $P^{\circ}_{O_2}(\max)$ the SiO pressure will drop and the loss of silicon will decrease to near zero since it must now diffuse through the solid silica layer. The SiO pressure that is defined by equation 12 is much lower than that defined by equation 7.

Resulting in the large drop in the SiO pressure when the critical oxygen pressure is reached.

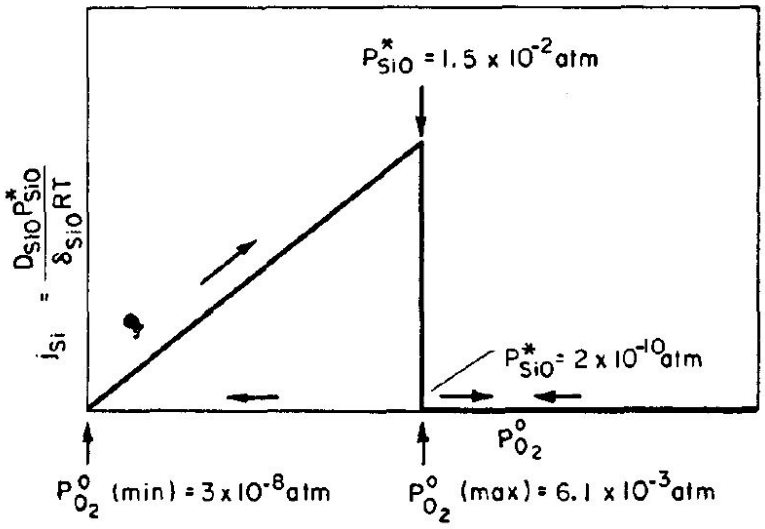

Figure 2--Loss of silicon from surface as a function of oxygen pressure. [1]

Several points to note about Wagner's model are that it was done looking at solid silicon instead of liquid. While much of the theory would be the same for liquid several changes would need to be made. First, is that gases (Si and SiO_2) other than SiO may be present due to the higher temperatures. Work by Gulbransen showed that at temperatures above 1400 ℃ that a significant SiO_2 pressure can develop as well as an increased Si pressure. [3] As the SiO_2 pressure increases the SiO partial pressure will decrease. As the Si partial pressure increases the amount of a reactive gas will increase and this gas will be able to react to both SiO and SiO_2. Secondly, Wagner assumed that the SiO_2 layer would be uniform across the whole surface. When dealing with a liquid surface it is possible that the surface will not be constant and that cracks could form more easily in the SiO_2 layer. The diffusion through these cracks would be much larger than the diffusion through solid silicon leading to an increase in the silicon loss.

2.1.2 Turkdogan Model

The other main model describing the oxidation rate of silicon was developed by Turkdogan et al. in 1963. [2] Like Wagner's model it was assumed that the reactions occur instantaneously and that the rate is determined by the mass transfer properties of the gas and metal. Additionally, Turkdogan's model is applicable to most metals not just silicon. Therefore, it does not take into account the presence of the reactive SiO gas, but is still said to give an accurate representation of the system. The presence of SiO gas in the silicon system complicates the calculations, but many of the basic principles of the model still apply. Figure 3 shows the model developed by Turkdogan.

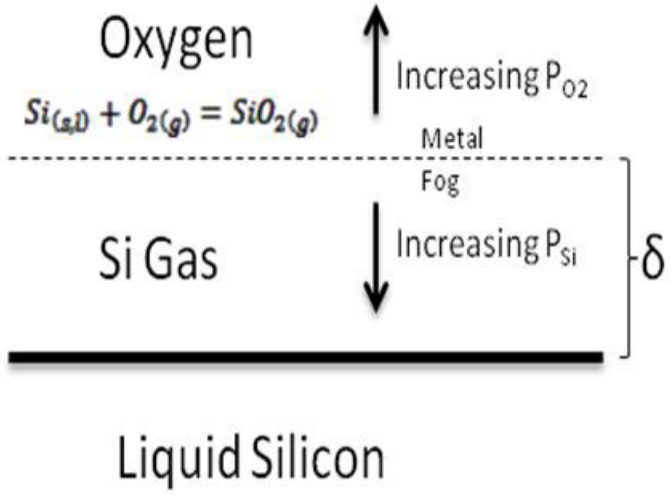

Figure 3--Schematic of the oxidation mechanism proposed by Turkdogan.

Turkdogan assumed that the oxidation of the metal occurred at a distance *δ* away from the surface. Under a steady state system the concentration of the metal vapor decreases moving away from the metal to the point *δ* and the oxygen content of the gas decrease from the bulk to the point δ as shown in Figure 4.

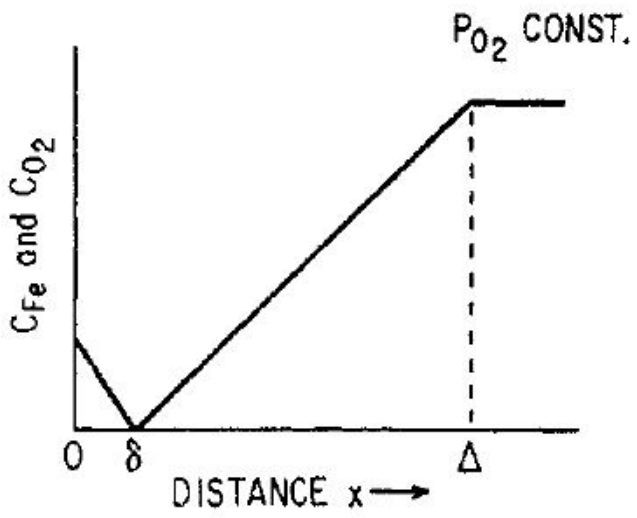

Figure 4--Schematic showing decrease in the pressure of both the metal vapor and oxygen. [2]

At *δ* Si vapor oxidizes straight to silica according to equation 2, the reaction produces a metal fog of silica. To calculate the silicon flux Turkdogan used Fick's first law of diffusion as a basis to find the rates of metal and oxygen transport to the point *δ*. Equation 13 and 14 show the flux of the metal and oxygen respectively.

$$J_{Si} = \frac{D_i}{\delta RT}(p^*_{Si} - p'_{Si}) \qquad \text{Equation 13}$$

$$j_{O_2} = -\frac{D_{O_2}}{(\Delta-\delta)RT}(p^{\circ}_{O_2} - p'_{O_2}) \qquad \text{Equation 14}$$

Where *Δ* is the boundary layer distance from the metal surface to the bulk gas and p'_{O_2} is the partial pressure at the point *δ*. For silicon the follow assumptions can be made: the two fluxes are equal, *δ* is much less then *Δ* and the partial pressures at *δ* are much lower than at the metal surface or bulk gas. Therefore, equations 11 and 12 can be simplified to equation 15.

$$J_i = -j_{O_2} = \frac{D_{O_2}}{\Delta RT}p^{\circ}_{O_2} = h\frac{\alpha p^{\circ}_{O_2}}{RT} \qquad \text{Equation 15}$$

Where *h* is the film mass transfer coefficient equal to $h = D_{O_2}/\Delta$ this definition neglects the effect of the oxide fog on the diffusion coefficients and *α* is number of gram-atoms of metal vapor needed to react with one mole of oxygen.

It can be seen that as the oxygen pressure is increased the loss of silicon will increase in a linear fashion. This is true until the active-passive transition where δ becomes zero and solid oxide forms on the surface. There are two restrictions on this model: maximum free evaporation rate cannot be exceeded and a minimum oxygen pressure must be maintained to have an oxide fog. The maximum free evaporation rate that cannot be exceeded is given by equation 16.

$$J_{max} = \frac{p_{Si}}{\sqrt{2\pi RTM_{Si}}} \qquad \text{Equation 16}$$

As the maximum rate is approached equations 13 and 14 become invalid for two reasons. First, is the metal surface is no longer saturated with the metal gas thus violation the initial boundary conditions used to solve Fick's law. Second, the distance δ approaches the mean free path between metal atoms. As the bulk oxygen pressure is increased eventually δ will go to zero and oxide will form directly on the surface. In other words the flow of oxygen inwards exceeds the flow of metal outwards. When this happens the partial pressure of the metal will decrease resulting in a decrease in the rate of metal loss.

The second restriction is that a minimum oxygen pressure is needed to get an oxide fog to form above the metal surface. This is not an issue unless at very low oxygen partial pressures.

From equation 15 it can be seen that the rate of vaporization is primarily dependent on the oxygen pressure and mass transfer coefficient. The effect of temperature can be neglected since the mass transfer coefficient is temperature dependent due to the diffusivity term and therefore the effect is nearly cancelled out. The mass transfer coefficient is given by equation 17.

$$h = 0.664 \left(\frac{D^4}{v_{O2}}\right)^{1/6} \left(\frac{v_g}{l}\right)^{1/2} \qquad \text{Equation 17}$$

Where D is the diffusivity, v_{02} is the kinematic viscosity v_g is the gas velocity and l is the length. The maximum oxygen pressure that the surface can remain free of oxide can be derived from equations 15 and 16 and is given as equation 18.

$$p^{\circ}_{O_2}(max) = \frac{p_i}{\alpha h}\sqrt{\frac{RT}{2\pi M_i}}$$ Equation 18

Therefore, for known gas flow conditions only the vapor pressure of the metal must be known to be able to calculate the maximum oxygen pressure that a bare silicon surface can be maintained (It is unclear of whether P_{Si} or P_{SiO} would give a more accurate result in the case of silicon), and the flux of the metal can be rewritten as equation 19.

$$J_i = \frac{D_i}{\delta}\frac{p_i}{RT}$$ Equation 19

The largest question that is raised when examining the Turkdogan model is how the presences of the SiO gas will affect the result. The assumption that equation 2 is the main oxidation equation is questionable since it requires a trimolecular reaction, of one silicon atom and two oxygen atoms, to occur. While this undoubtedly happens it occurs much less often than a bimolecular collision. If the reaction is assumed to go through multiple steps that include equations 1 and 4 this becomes more plausible and equation 2 can be said to be the overall reaction. Additionally, this could help to eliminate the problem of the SiO gas.

2.1.3 Hinze and Graham

In order to overcome the discrepancies between the Wagner and Turkdogan models Hinze and Graham undertook a series of experiments on silicon and silicon carbide in 1976. [(4)] They used thermogravimetric analysis to look at the effect of temperature and oxygen pressure. The results were not conclusively able to support either model; however, the results supported many aspects of the Wagner's theory. The largest difference from the two models that was found was that that the transition from active to passive oxidation occurred in two stages not the one as predicted by Wagner and Turkdogan.

The starting point was the same as Wagner and Turkdogan, a low oxygen pressure and a bare solid silicon surface. As the oxygen pressure was increased a certain pressure was reached where small islands of silica formed on the surface. With a further increase in the oxygen pressure the islands were found to grow vertically from the surface to

form silica whiskers this was called stage one oxidation. Eventually as the oxygen pressure was increased, an oxygen pressure was reached and the entire surface became passivated in what is called the stage two critical pressure. This is shown schematically in Figure 5 below.

Evidence was found that supported the Wagner model; by looking at the activation energies it could be seen was that the value for second stage oxidation is approximately 83 kcal/mol this is agrees well with the value of 83 kcal/mol that was found by Zmbov *et.al.* for equation 4 this means that it the SiO transport from surface that was predicted by Wagner is the likely reaction mechanism rather than Si vapor.

The mechanism for the formation of the silica whiskers that was proposed by Hinze and Graham is that as the oxygen pressure is increased the equilibrium SiO pressure will be reached. At this point silica forms on the surface as small islands rather than a continuous sheet. The silica will grow vertically from the surface for two reasons. First, is that the silica will act as a nucleation site promoting further silica formation via equation 4. This growth in increased by the fact that the oxygen partial pressure increases from near zero at the surface to the bulk concentration away from the surface. This means as a SiO molecule diffuses away from the surface it will encounter an increasing oxygen potential thus increasing the likelihood that it will react to form silica on the existing silica surface. This results in a vertical growth of silica rather than the horizontal.

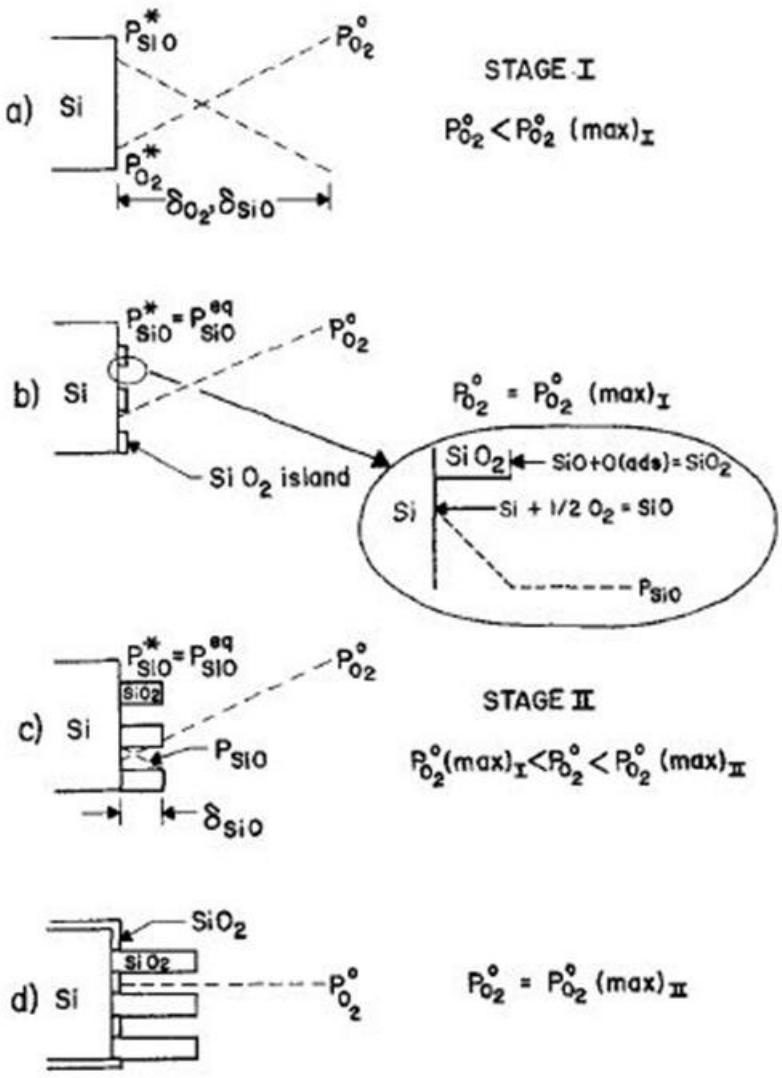

Figure 5-Oxidation mechanism proposed by Hinze and Graham. [4]

Eventually though the oxygen pressure is increased enough that the outward diffusion of SiO cannot keep up with the inward diffusion of oxygen and solid silica covers the entire silicon surface resulting in complete passivation. Even though the mechanism is different it was found that the rate of oxidation still compared well with the rate of oxygen supply to the surface indicating that it is still under a mass transfer regime. The values for second stage passivation are in near agreement with those of Wagner for the active to passive transition.

In order for the surface to remain bare after the first stage critical oxygen pressure has been reached the removal of SiO must increase to continue to match the increasing flux of oxygen towards the surface. The pressure of SiO is fixed by equilibrium with the silica formed on the surface therefore the boundary layer thickness must decrease as shown in equation 19. Therefore, at the tip of the whisker some of the oxygen is consumed to produce silica resulting in a decreased boundary layer thickness. This reaction is similar to the Turkdogan model where oxygen is consumed above the surface. According to equation 19 with a decrease in δ an increase in the flux will occur and active oxidation will continue until the stage two critical oxygen pressure is reached according to equation 9 developed by Wagner.

2.2 Effects of Calcium and Aluminum on Silicon Oxidation

Calcium and aluminum are considered to be the two main impurities in MG-Silicon. When tapped from the furnace they typically have a concentration of 0.2% calcium and 0.6% aluminum. During ladle refining the concentration is reduced to 0.02% calcium and 0.15% aluminum. [5] The effects of calcium and aluminum on the oxidation rate of silicon are still not completely understood.

Calcium and aluminum will have low partial pressures above the silicon due to their low concentrations in the melt and their low vapor pressures compared to SiO. This means that under an active oxidation regime (where oxidation occurs in the gas phase) the effects will be limited. However, during passive oxidation the oxide layer will act like a slag and the calcium and aluminum with have a more pronounced effect on the oxide layer and oxidation rate. [6] This is true regardless of which oxidation model is being used since both models require the metal to leave the surface as a gas; either before or after oxidation has occurred and the low vapor pressure will hamper that in comparison to silicon.

Since it is assumed that at the flow rates and oxygen pressure that the experiments will be carried out at the silicon surface will be at least partially passivated the interaction between the melt and oxide layer are of importance. Therefore, the SiO_2-Al_2O_3-CaO

slag system will be briefly examined to help understand how the calcium and aluminum may be distributed between the metal and oxide.

The distribution coefficients for calcium and aluminum in regards to the slag system are well known and studied. Given that the activity of the silicon is assumed to be much higher than the calcium and aluminum activity it can be said that once an oxygen atom is introduced to the system it will react to form silica. This silica will then react with aluminum and calcium if the silica interacts with a calcium or aluminum atom. Shown by equations 25 and 26.

$$3SiO_{2(s,l)} + 4Al = 2Al_2O_{3(l)} + 3Si_{(l)} \quad \text{Equation 25}$$

$$SiO_{2(s,l)} + 2Ca = 2CaO_{(l)} + Si_{(l)} \quad \text{Equation 26}$$

The concentration of calcium and aluminum in the metal can then easily be written as equations 27-28. The *k* values have been determined and are given in table 2. Using this data the concentration of calcium and aluminum dissolved in the melt can be calculated and are shown in Figure 6 as an isoconcentration curve for 1550℃. [5] It can easily be seen on the figure that as the concentration of calcium and aluminum is decreased in the melt the equilibrium concentration in the slag must also change. Line A-B on Figure 6 is an example of this change. Additionally, it has been found that the oxygen efficiency is dependent on the concentration of calcium and that as the concentration of calcium is depleted the efficiency will be decreased. [5]

$$[\%Al]_{Si} = k_{Al,Si} \times \frac{1}{\gamma_{Al}} \frac{(a_{Al_2O_3})^{0.5}}{(SiO_2)^{0.75}} \quad \text{Equation 27}$$

$$[\%Ca]_{Si} = k_{Ca,Si} \times \frac{1}{\gamma_{Ca}} \frac{(a_{CaO})}{(SiO_2)^{0.5}} \quad \text{Equation 28}$$

Table 2 Published k values for equations 25 and 26. [5]

	1550℃	**1600℃**
[%Al]	0.097	0.120
[%Ca]	0.0086	0.012

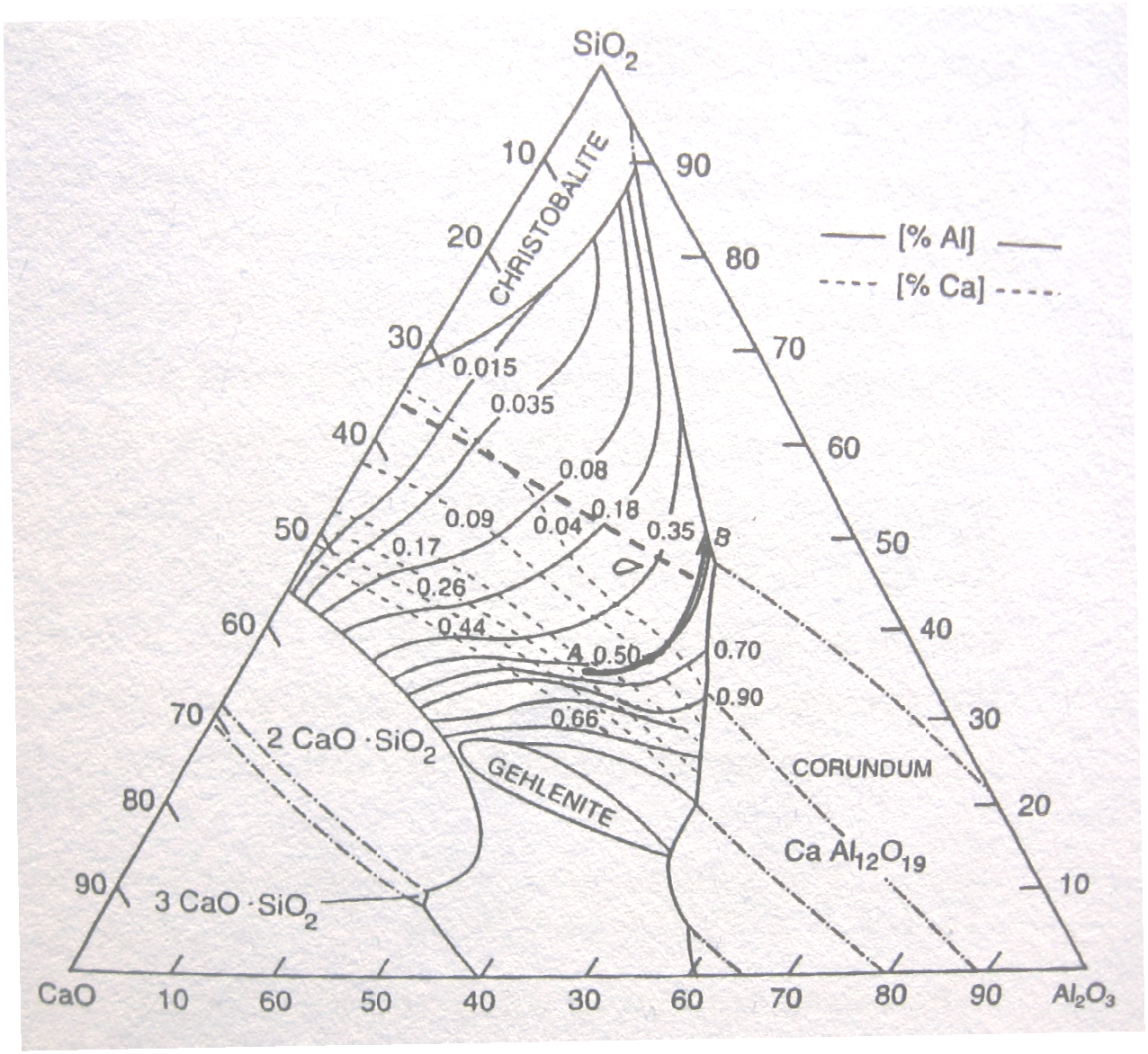

Figure 6--Isoconcentration curves for aluminum and calcium at 1550°C. [5]

2.3 Industrial Measurements

Measurements of the silica fuming rate were carried out at Elkem Salten Plant in Norway. [7] A laser particle analyzer was used to measure the amount of silica fume formed during refining by gas purging. Table 3 shows the results of these measurements.

Table 3 Results of industrial fume measurments carried out by Næss at Elkem Salten [7]

Measurement #	Area of exposed Si (m^2)	SiO_2 (kg/h)	SiO_2 (kg/h m^2)	SiO_2 (moles/s m^2)	Max (kg/h)	Min (kg/h)	Calc. SiO_2 from bubbles (kg/h)
1	0.45	4.4 (0.7)	10 (1)	0.046 (.007)	5.9	3.0	0.082
2	0.31	5.1 (0.6)	16 (2)	0.076 (.009)	6.7	3.4	0.11
3	0.30	2.9 (0.3)	9.5 (0.9)	0.044 (.004)	3.8	2.0	0.020
4	(0.37)	5.1 (0.3)	13.9 (0.9)	0.064 (.004)	6.7	3.6	0.11
5	(0.37)	3.9 (0.3)	10.5(0.8)	0.049 (.004)	5.1	2.7	0.023
6	(0.37)	2.5 (0.2)	6.7 (0.5)	0.031 (.002)	3.2	1.7	0.022

These measurements were taken during oxidative ladle refining. During which the gas is purged from the bottom of the ladle containing liquid silicon. It was found that the primary oxidation occurred on the surface of the melt and was dependent on the exposed surface area and flow rate of the gas.

Additionally, silica dust samples were collected for particle size and compositional analysis. The samples were place in an SEM and analyzed with EDS. It was found that the particles were spherical and composed entirely of SiO_2. The size distribution of the particles is presented in Figure 7. It can be seen that a majority of the particles are less than 0.05 µm in diameter.

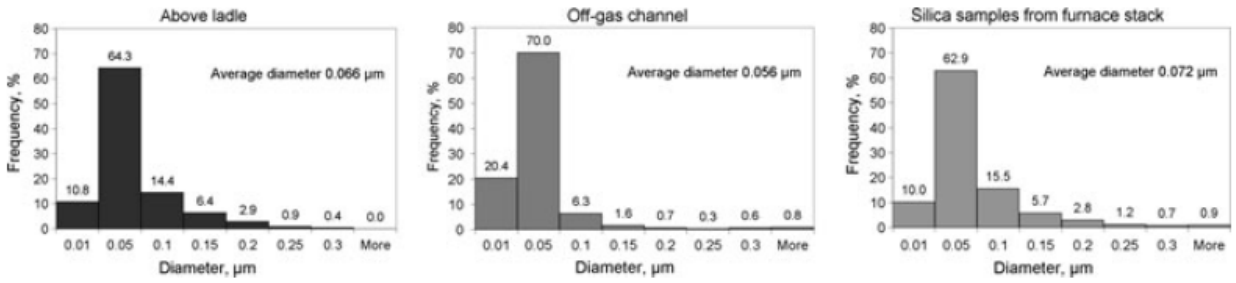

Figure 7--Particle size distribution from industrial measurements at Elkem Salten. [7]

2.4 Boiling Point Model

The tendency of a particular element to report to the silica fume, Si metal or slag can be predicted with reasonable certainty based on a few key properties. In the in the boiling

point model developed by Myrhaug and Tveit the distribution of an element is determined by its boiling point. [8] As shown in Figure 8. The boiling point model was developed for emissions from the FeSi furnace. When examining the refining of silicon the model is not as ideal. This is because during refining the temperature is lower and a slag covers the silicon surface.

To examine the distribution of impurities during refining samples of the fume from industrial ladles were taken by Næss in 2010 and analyzed by ICP-MS to see how they compared to the boiling point model. [9] For the most part the emissions from the refining stage were in agreement with the boiling point model. The results are shown in Figure 9.

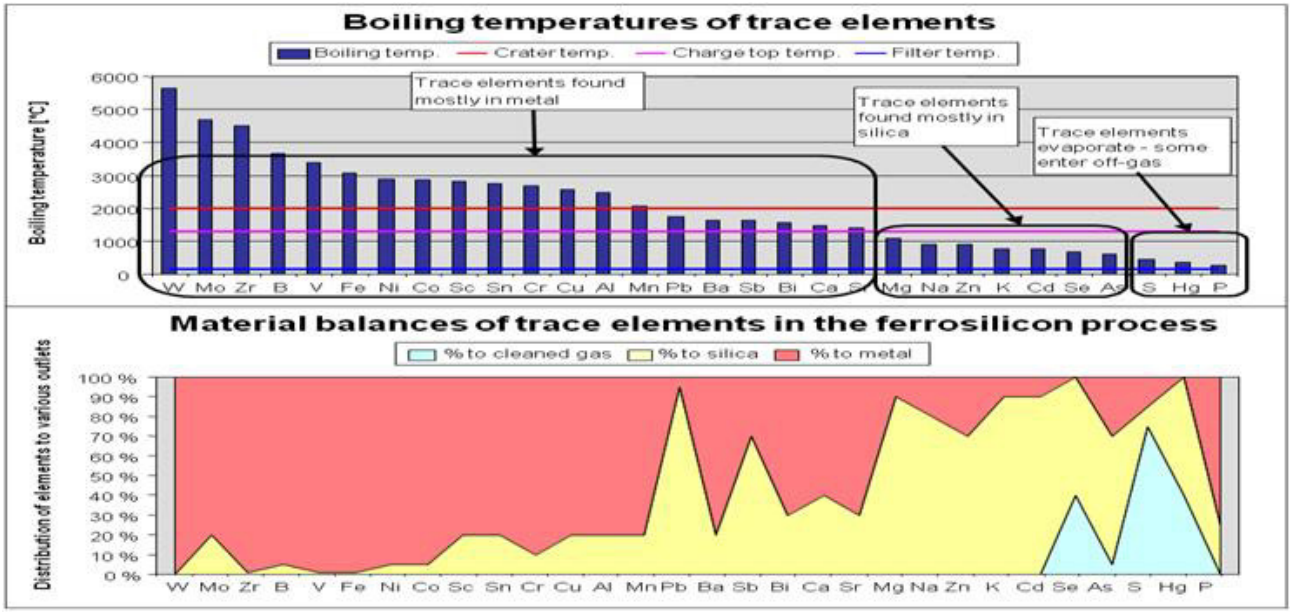

Figure 8--Boiling Point model.

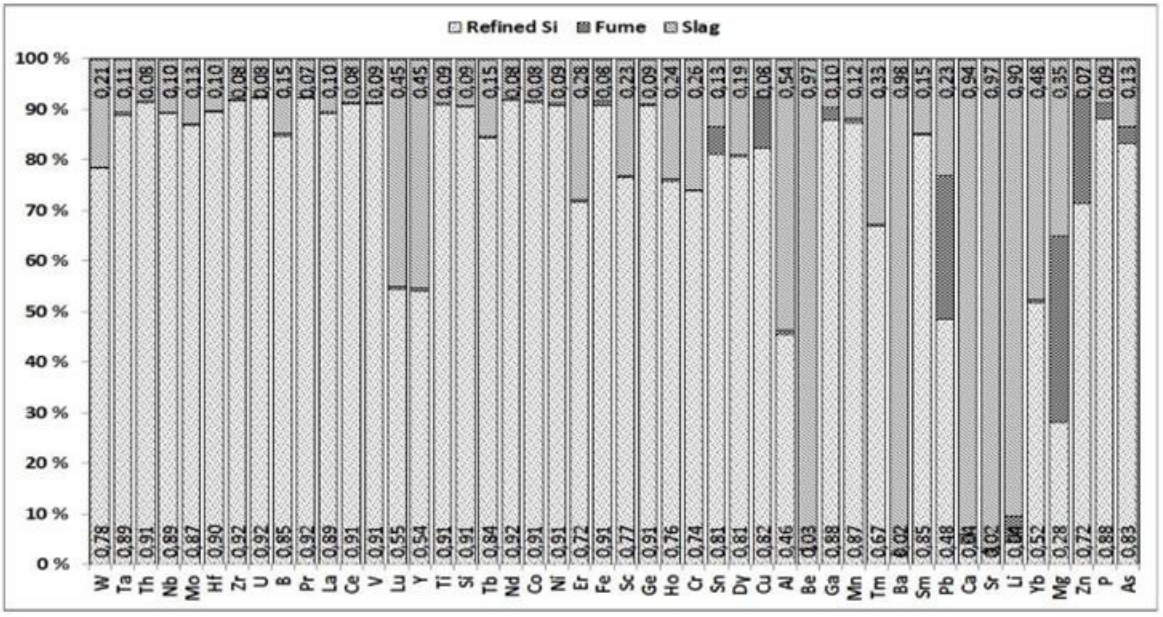

Figure 9--Results of measurments taken industrial refining.

Since the primary elements of the system are calcium and aluminum these two will be examined more closely. According to both the boiling point model and the work by Næss, calcium and aluminum will primarily report to the metal and slag phase. Both will be found in the fume, but in small quantities. Both elements have higher oxidation potentials than silicon so they are typically assume to be found in the slag phase. Other elements that can be expected to be found in the fume are Pb, Mg and Zn. However, percentage of these elements in the starting melt is much lower than the calcium and aluminum and will likely be found in smaller amounts in the fume.

3 Experimental

3.1 Continuation of Experiments in Muffle Furnace

In order to clarify the some of the results from the project work on the effects of aluminum and calcium on the oxidation of liquid silicon further analysis of the samples from the experiments was made with EPMA. [10] In these experiments a small chip of silicon was placed in an alumina crucible and oxidized at four different times and two temperatures the mass change of the samples was then plotted with time. This allowed the affects of both time composition and temperature to be seen. Since the original series with 0.5% Ca did not reveal reliable results that series was rerun.

The oxidation of the 0.5% Ca samples was done with the same procedure as was described in the project report “Oxidation Kinetics and Mechanisms of silicon and Si-Al-Ca alloys,” [10] however, a brief summery is presented here. A chip of electronic grade silicon that was alloyed to have 0.5% Ca was placed in an alumina crucible. The chip size varied from 1.35-1.52 grams. A “Kanthal Super Rapid High Temperature Furnace” was used shown in Figure 10; this furnace is a refractory lined and open to an air atmosphere. It is assumed that the circulation within the furnace is great enough that the atmosphere does not change during the course the experiment.

Figure 10-- Muffle furnace used for oxidation experiments.

The furnace was heated to 1550℃ prior to loading the sample. The weight of the silicon chip and the silicon chip plus the crucible was taken on an electronic balance with an accuracy of 0.1 mg. the sample and crucible was then placed in the furnace. Time began from the moment the door was closed on the furnace. During the loading procedure the temperature would drop to around 1300℃, but would recover to 1550℃ within one minute. Samples were oxidized for 20, 40, 60 or 90 minutes. After the required time had elapsed the sample was removed from the furnace and allowed to cool in open air down to room temperature. During cooling cracks appeared in the alumina crucible due to the expanding silicon and high cooling rate. Once cooled the sample and crucible was weighed again. The mass difference from before and after oxidation was calculated for each of the samples and then plotted to see how it changed with time. The sample was then broken free from the crucible. This could be done without damaging the sample or oxide layer since silicon does not wet alumina and the two were poorly attached. The sample was then mounted in an epoxy resin and examined by EPMA to understand how the oxide layer composition changed with time.

3.2 Experiments in IF75 Furnace

A series of experiments was planned to study the effect of airflow rate on the oxidation rate of liquid silicon in a medium scale induction furnace. The basic plan was to blow air at different rates (LPM) onto the surface of liquid silicon creating a silica fume and measure the mass loss of silicon or the mass of silica fume produced. A filter was employed to capture the silica fume for analysis with SEM and EDS. Since this work concerns the refining of silicon both refined and unrefined MG-silicon will be tested to see if the metal composition has any impact on the silica flux. In the industrial measurements it was shown that the quantity of oxygen is limiting and not the velocity though it will have an effect on the diffusion boundary layer. Therefore the gas flow will be defined in liters per minute (LPM)

3.2.1 Experimental Setup

The experimental setup is shown in Figures 11 and 12. The system consists of a graphite crucible and lid; placed in the lid was a S-type thermocouple inside a graphite thermowell, a graphite air lance with an inside hole diameter of 5mm and an exhaust port that was connected to the water cooler and dust collector. The lance is placed in the center of the lid with the thermocouple and exhaust port on either side. The dust filter had a maximum temperature of 280℃ therefore the dust and gas were cooled prior to reaching it. To do this the exhaust is passed through stainless steel pipe with a 12 mm inside diameter that was water cooled by a copper tube wrapped around the outside of the pipe. The total length of the pipe from the lid to the dust collector is 300 mm to allow adequate cooling for the gas. Additionally, by cooling the gas all to this temperature the SiO gas becomes unstable and is oxidized to SiO_2 and trapped in the filter. Once cooled the exhaust enters into the dust collector. The dust collector was a stainless steel box with a fiber filter. The filter material was “Gore Acid Resistant Fiberglass” that is the same material as the baghouse filters employed in many industrial silicon plants. No minimum particle size is given for the filter, but during the experiments no silica fume was found to exit the filter so it assumed that all fume was captured by the filter. Filtered compressed air was used and the flow was measured at room temperature with a rotameter. The crucible used was composed of graphite and

measured 40 cm high and an outside diameter of 15 cm. The inside diameter was 11.4 cm giving a total surface area of 102.1 cm^2 assuming a flat silicon surface. All graphite parts are assumed to react with the silicon or air at high temperatures and must be taken into account during the final mass balance calculations. The crucible, thermowell and lance were all consumed during the course of a single experiment and new ones were used each time. The lid was able to be reused for up to five experiments before the loss to CO gas necessitated its replacement.

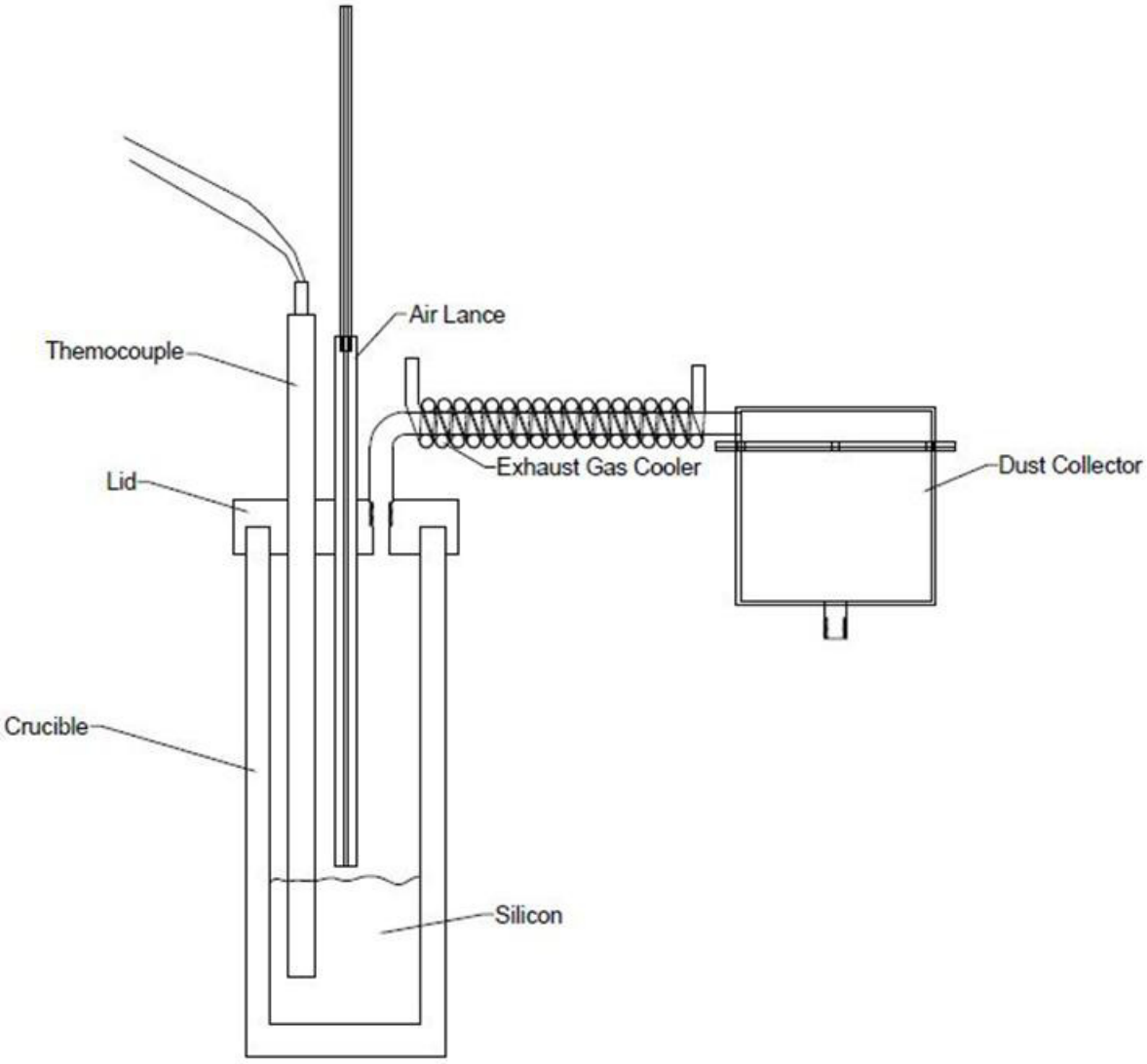

Figure 11--Experimental Setup for medium scale induction furnace.

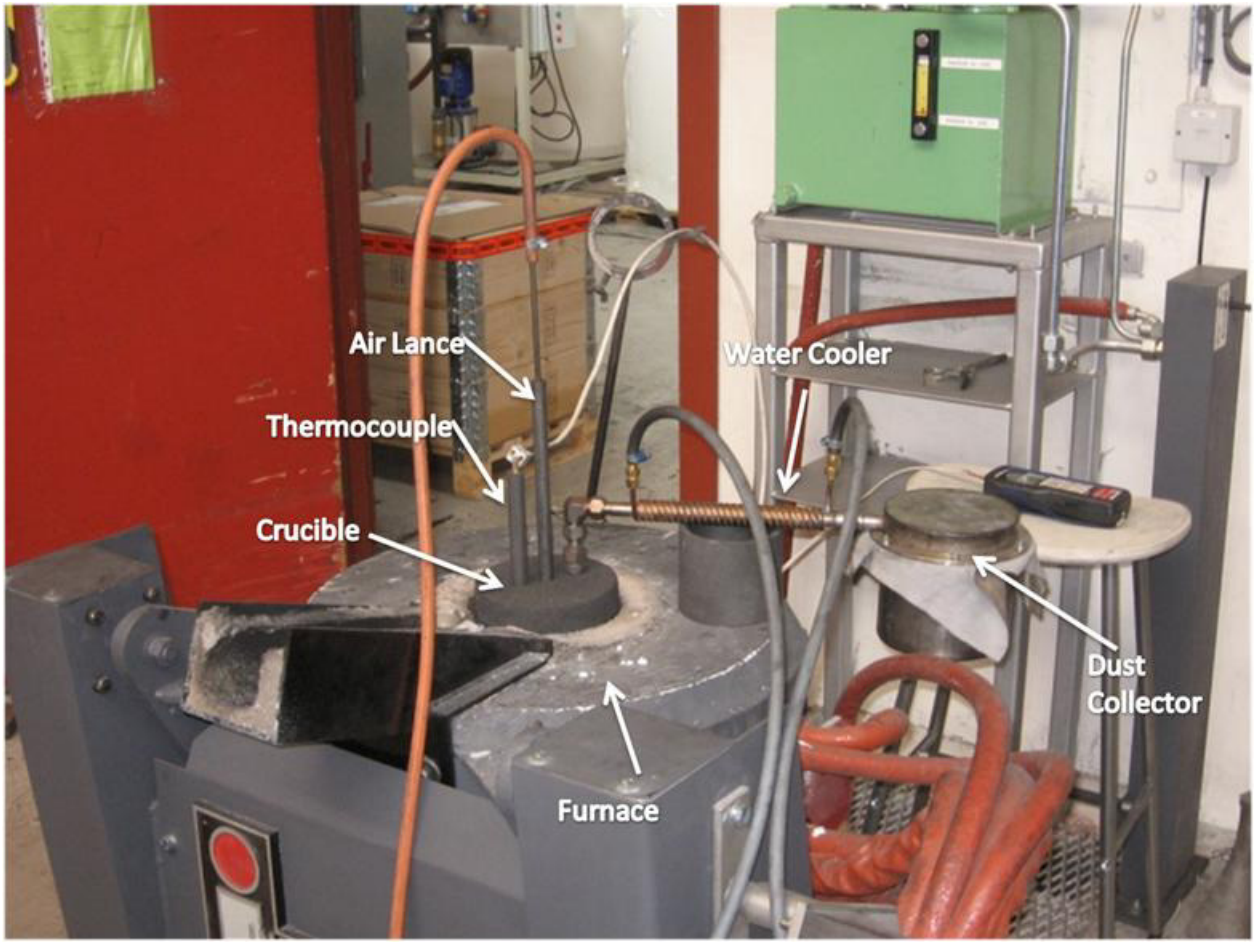

Figure 12--Experimental setup with furnace, crucible and dust collector.

The furnace used was an IF 75 induction furnace produced by Inductotherm. This furnace is capable of quickly heating the crucibles and the temperature is read through an external thermocouple and reader. The power is then adjusted to increase or decrease the temperature.

The velocity of the air over the surface of the silicon is difficult to define as it is dependent distance from the center of the crucible. The maximum velocity at the tip of the lance can easily be calculated from the flow rate and lance diameter; the velocity of the gas then decreases as it moves outward from the center. Additionally, it was considered to be turbulent flow at all flow rates tested due to the geometry of the system. Table 4 gives the tested flow rates and the maximum velocity obtained. The rotameter used to set the airflow was at room temperature therefore the gas velocity

when it reaches the silicon surface would be higher than originally calculated. The exact gas temperature is not known. To estimate the velocity a temperature of 1000℃ was assumed, and based on this estimation the new velocities are given in the 3rd column of Table 4.

Table 4 Airflow and Max Velocity used for experiments.

Air Flow (LPM)	Max Air Vel. Cold (m/s)	Max Air Vel. Hot (m/s)
1	0.85	3.95
3.5	2.97	13.85
5	4.24	19.79

The surface topography of the liquid silicon during blowing is also unknown. The surface is expected to be at least partially passivated during blowing; however, an open eye may exist at higher flow rates.

Refined metallurgical grade silicon was used for all the experiments. When unrefined metallurgical grade silicon was required the refined silicon was doped with 1% Al and 0.5% Ca. 1100 series aluminum was used for the aluminum doping and a CaSi containing 30% Ca, 60% Si 0.3% Al 0.52% C was used to achieve the needed calcium level. The aluminum and CaSi were added to the top portion of the charged crucible. The stirring in the crucible caused by the induction furnace was assumed to be enough to insure a homogeneous distribution of the calcium and aluminum.

3.2.2 Experimental Procedure

Due to the tendency of the dust to be deposited on all surfaces it was important to weigh all parts of the collector so that a mass balance could be completed. The first step, therefore, was to weigh all of the individual components. Next, between 2250-2400 grams of silicon was charged in to the crucible. Once melted, the silicon charge resulted in a total bath depth ranging from 8.56-9.15 cm assuming a liquid density of 2.57 g/cm^3. The thermowell was set in place at the same time as the silicon and was placed so the tip was approximately 4 cm from the bottom of the crucible. The total

mass of the crucible, silicon and thermowell was recorded the lid was placed on and it was set into the furnace. Graphite wool was placed between the crucible and the furnace refractory to help protect the furnace. The filter was then weighed and placed in the filter box. The filter box and cooler tube were then threaded to the lid. Once again the starting mass of all the parts was noted. The lance was then placed into the lid, but not lowered to its required depth. The air was then turned on to test for leaks, and then was turned off until the target temperature was reached. The furnace was then turned on and set to 15 kW to heat the crucible up to 1550°C. This power setting was used for all experiments and it was only changed when the target temperature was reached. This was done to keep the graphite losses to CO the same across all experiments. In total it took approximately 70 minutes for the furnace to get to 1550°C. Once at the required temperature the power was set to between 12.5 and 14 kW in order to maintain the 1550°C. During the experiment the temperature would vary from the set point by ±25°C.

The lance was then lowered so the tip was 2-3 cm above the surface of the melt and the air was turned on and set to the desired flow rate. During the experiments at the higher flow rates the buildup of silica fume in the exhaust tubes would cause a reduced diameter and an increased pressure in the crucible. Since the rotameter is designed and calibrated to operate at 1 atm this pressure increase caused the reading on the rotameter to change over the course of the experiment. Regardless, once the air flow was set at the start it was left unchanged. The change in the value displayed on the rotameter was noted so the pressure change within the crucible could be calculated if needed. At the higher flow rate the cooling tube became blocked after 20 minutes of blowing therefore this time was used for all experiments. After the blowing was completed the air flow and furnace were shut off. Within fifteen minutes of shutting the furnace off the crucible was removed from the furnace. The lid and lance were then taken-off the thermowell was stuck in the silicon and could not be removed. After the system was allowed to cool for several hours, the final mass of all the parts was recorded and used to calculate the mass change. Finally, fume samples from the filter, cooling tube and bottom side of the lid were collected for analysis with the SEM.

3.2.3 Analysis Methods

Two methods were used to examine the results. First, is mass loss and gain. There is expected to be a mass loss of silicon from the crucible during the experiment, therefore the mass of the crucible and silicon will be measured before and after each experiment. This means the loss of graphite to CO was also be recorded. Additionally, in the filter and cooling tube silica fume would build up and a mass gain was seen. These two mass changes were related to the flow rate and metal composition.

Secondly, the fume was examined by SEM (Scanning Electron Microscope) and EDS (Energy Dispersive Spectroscopy) to determine how the particle size and composition changed with flow rate and metal composition. For SEM analysis the fume samples were affixed to conducting carbon tape attached to the head of brass bolts. Six of these bolts could then be loaded in the SEM at a time. The SEM used was a Zeiss Ultra 55 Limited Edition field emission microscope. Due to the charging nature of silica fume the accelerating voltage was set to 5 kV and a working distance of 4-5 mm. A Bruker EDS system was used for the chemical analysis with a working distance of 10 mm and an accelerating voltage of 20 kW. A particle size distribution was carried out on the images gathered in the SEM. The images were analyzed and measured with the program ImageJ.

4 Results

The results have been broken into two sections the results from the muffle furnace experiments will be presented first followed by the results of the induction furnace experiments. Included in the results are the mass change, SEM images, EDS scans and calculated mass balances.

4.1 Muffle Furnace Experiments

As a continuation of the work done for the semester project the oxidized silicon samples were analyzed with the EPMA to get a more accurate understanding of how the calcium and aluminum were distributed and the effect they had on oxidation of silicon. Below are the results from the 1% Al, 0.5% Ca and 1% Al-0.5% Ca samples that were oxidized at 1550℃.

4.1.1 1% Al

The oxide layer on the samples with 1% Al was the most uniform of the three different compositions. The oxide layer formed quickly on the surface and allowed the sample to retain its original shape even though the silicon was liquid. The layer was found to be composed of silicon, aluminum and oxygen. The ratios of the three lead to the conclusion that the oxides present are Al_2O_3 and SiO_2. The composition of the layer shows no significant changes with regards to time and position in the layer. The oxide layer consisted of 93.8% Al_2O_3 and 6.2% SiO_2 on average. Figure 13 shows the oxide layer. Since both the composition and mass change were not affected with time it can be concluded that the oxide layer it formed within the first 20 minutes and passivated the silicon reducing further oxidation.

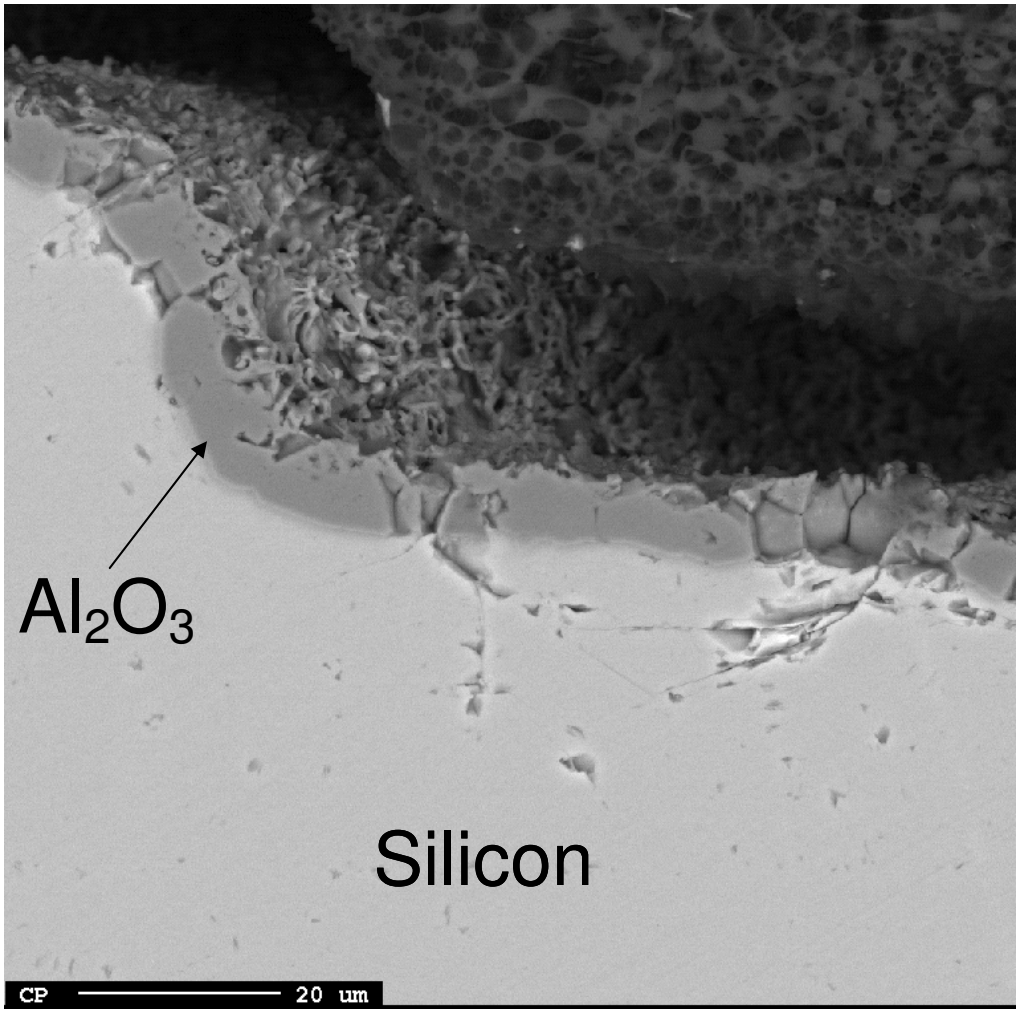

Figure 13—EPMA micrograph of the oxide layer on a 1% Al sample

4.1.2 0.5% Ca

The 0.5% Ca at 1550℃ experiments that were rerun to obtain more consistent results than the initial series. Below in Figure 14 are the percent mass change of the 0.5% Ca samples both from the original series and the rerun. Due to the scattering of the data it is difficult to draw any solid conclusions. All samples had between 8.8 and 19.1 % mass gain.

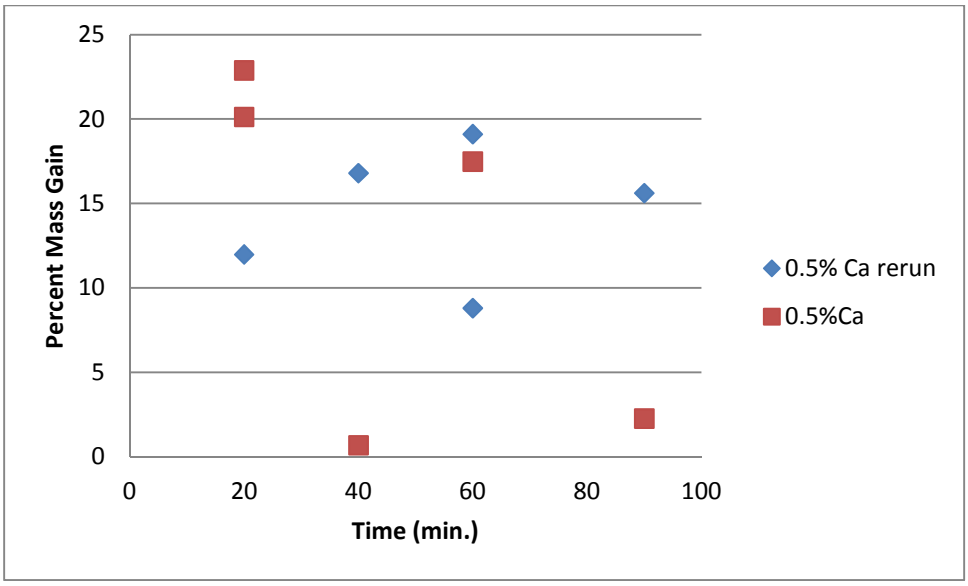

Figure 14--Percent mass change from 0.5%Ca samples

Examination of the samples with the EPMA yielded several interesting results. First, as with the original 0.5% Ca samples contamination from the alumina crucible was found. Within the oxide layer three clear phases were present; an Al_2O_3-CaO-SiO_2, a SiO_2 and a pure Si phase shown in figure 15. Note that no points were found that contained CaO without Al_2O_3 being present. The pure Si phase appeared as small droplets less than 50µm in diameter. These droplets were present at all times. The Al_2O_3-CaO-SiO_2 and SiO_2 phases made up the bulk of the oxide layer. The Al_2O_3-CaO-SiO_2 phase was found primarily near the metal oxide interface though it was occasionally found in the near the top of oxide layer. The Al_2O_3 and CaO were found in nearly equal amounts ranging from 8-16.8 at% with the remainder being SiO_2. The oxide layer appeared to be stable showing no changes in composition with time.

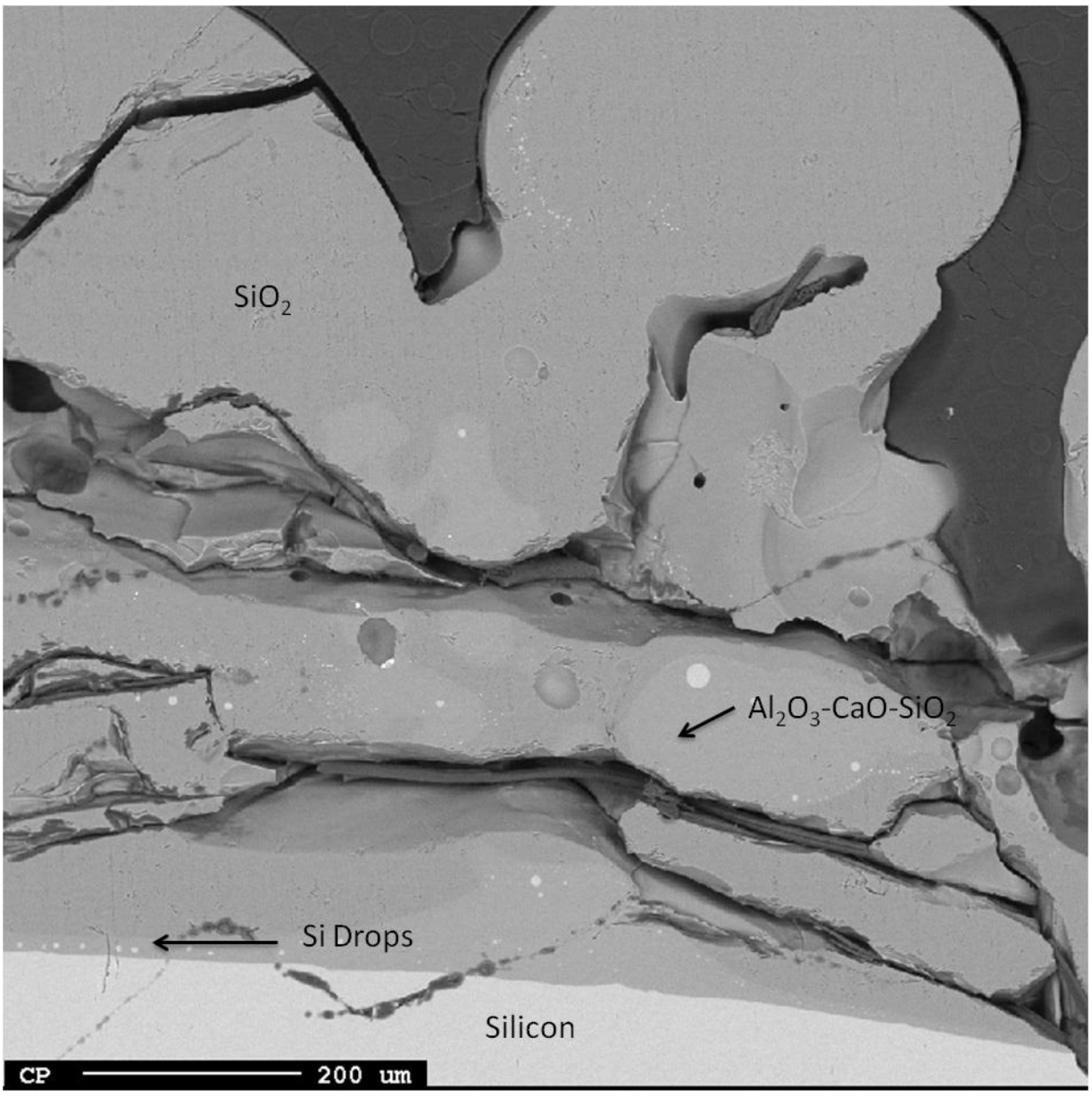

Figure 15--Oxide layer on 0.5% Ca 90 min. Sample (cracks due to cooling).

4.1.3 1%Al-0.5%Ca

The oxide layers in the 1% Al-0.5% Ca samples were the most complex and the only ones that showed a change in composition with time. Two phases were observed in these samples. One containing near equal parts Al_2O_3 and CaO with high SiO_2 percentages; the second was made up of primarily Al_2O_3, but contained small amounts of SiO_2. In the phase containing primarily Al_2O_3 an increase in SiO_2 was seen with

increasing time. The composition of the two phases are shown in Figures 16 and 17. The morphology of the phases also changed with time. Initially the high Al_2O_3 phase had a plate like appearance. With time the edges softened and grew together as can be seen in figures 18 and 19, showing the 20 and 90 minute samples.

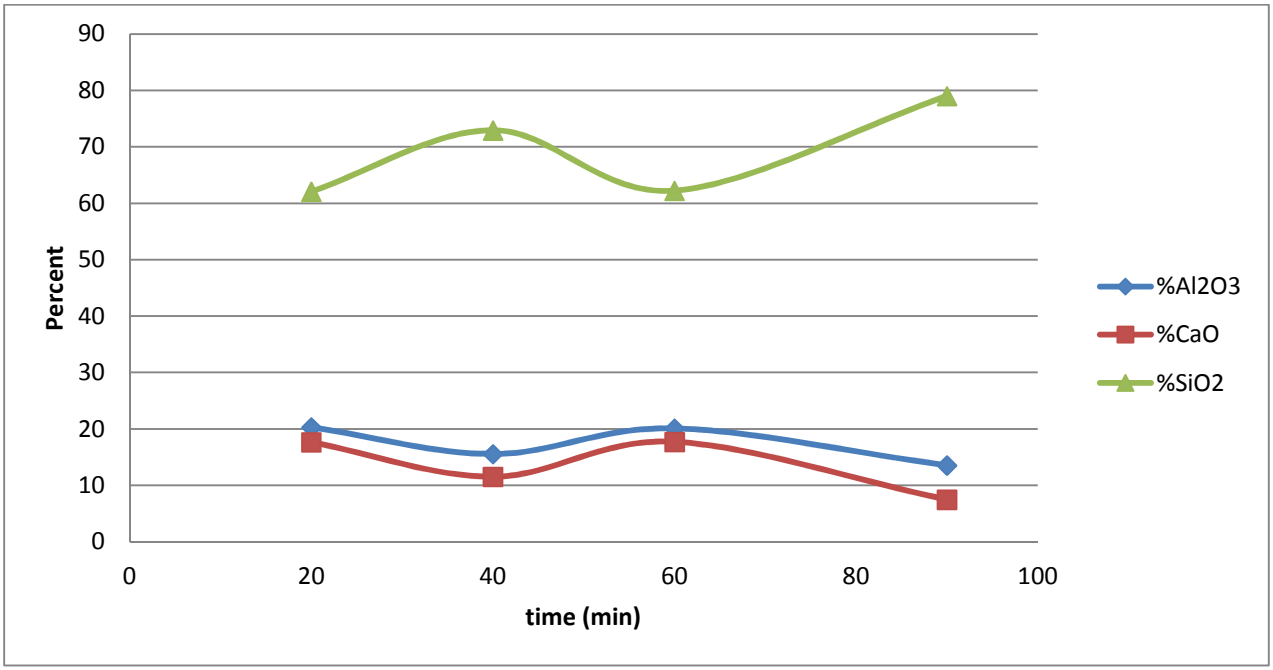

Figure 16--Composition of high SiO_2 phase in 1% Al-0.5% Ca samples (light phase figures 18 and 19).

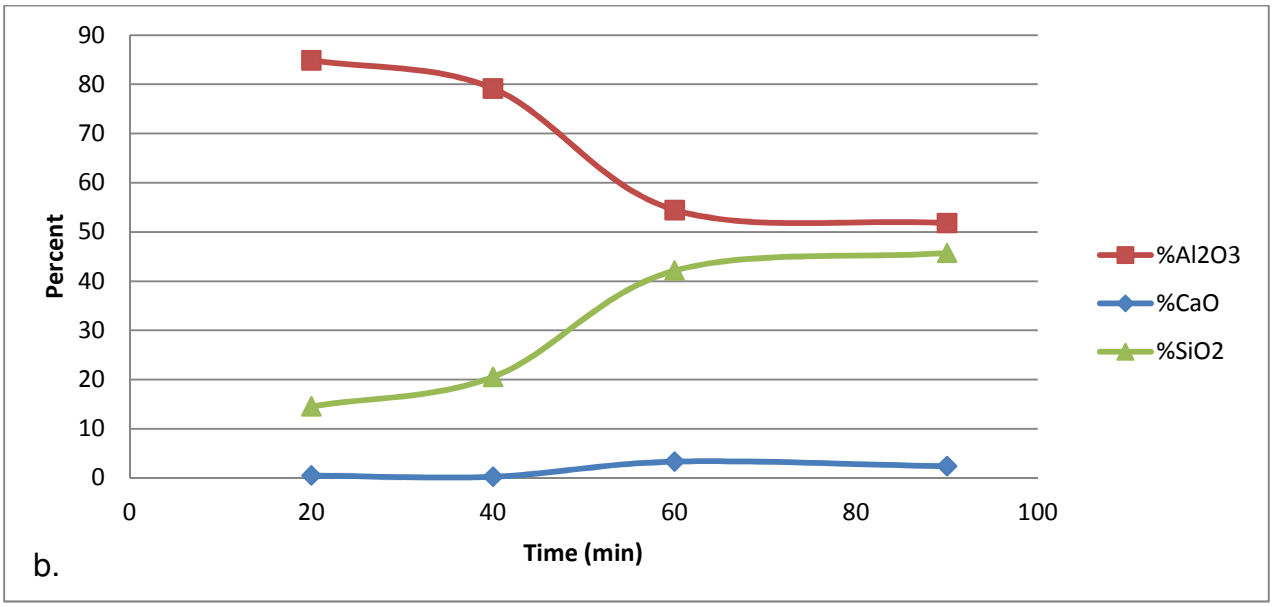

Figure 17 --Composition of high Al_2O_3 phase in 1% Al-0.5% Ca samples (dark phase of image 18 and 19).

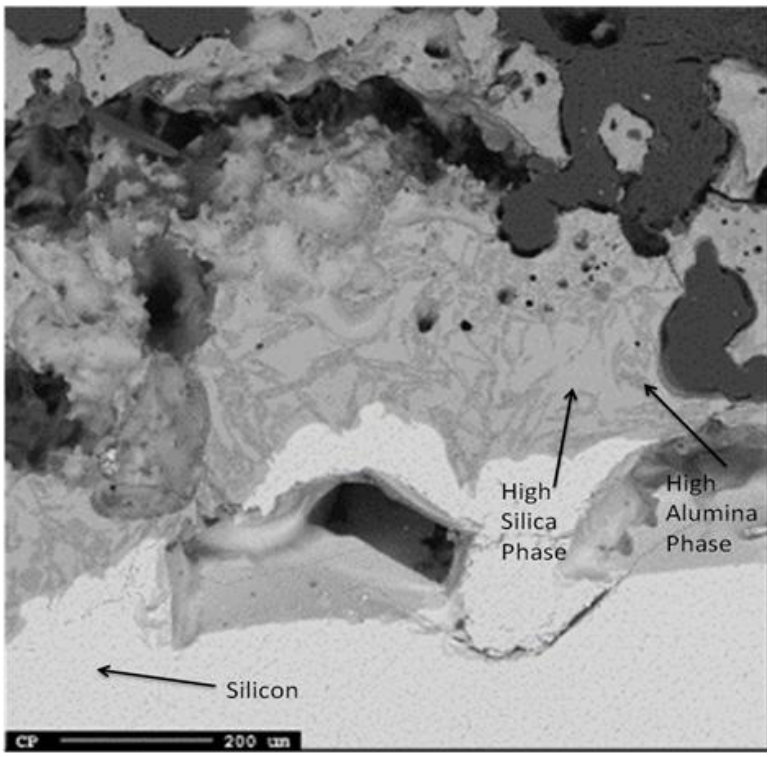

Figure 18--20 minute 1% Al-0.5% Ca sample.

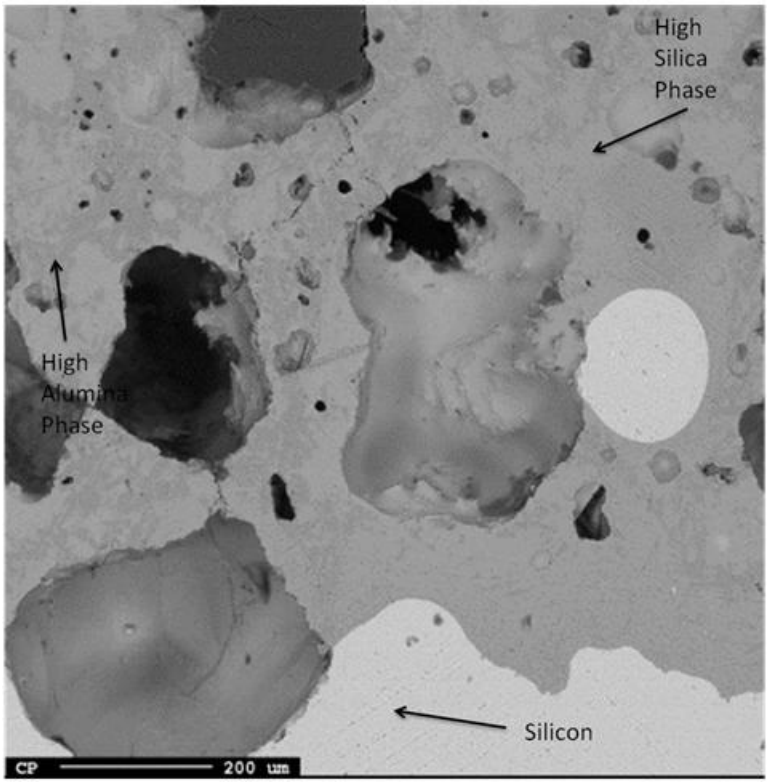

Figure 19--90 minute 1% Al-0.5% Ca sample.

4.1.4 Comparison of 1% Al, 0.5% Ca and 1% Al-0.5% Ca

It can be seen in figure 20that the addition of 0.5%Ca had the largest mass change followed by the 1% Al-0.5% Ca then by the 1% Al samples all the samples had a higher mass change then pure silicon according to the work by Lapointe. [11] In a similar set of experiments Lapointe found the mass change to be less than 2.5%. This is close to the results from the 1% Al.

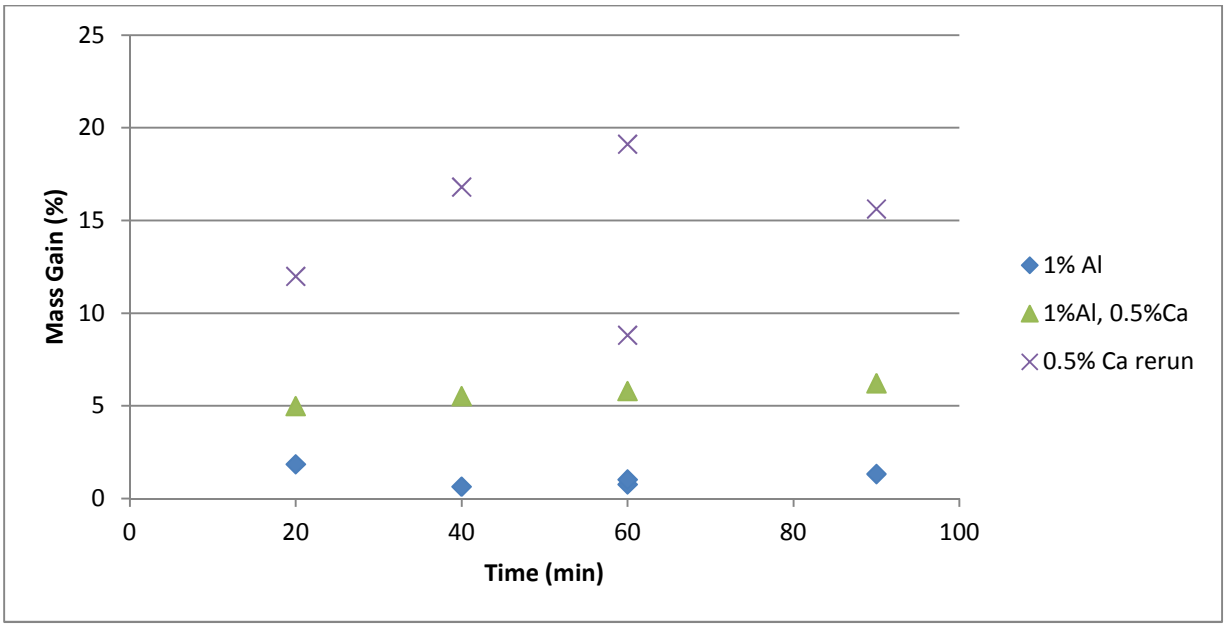

Figure 20--Mass change of all samples at 1550℃.

4.2 Induction Furnace Experiments

4.2.1 Mass Change

In addition to the measured mass loss or gain from the crucible and filter. The mass of the silica fume that accumulated in the tubing from the crucible to the filter was estimated. The mass loss from the crucible is given in Figure 21. This shows the total mass lost from the crucible, thermowell and silicon. It was not possible to separate the crucible, thermowell and silicon after the experiment was run, therefore, the mass loss must be presented as a total of all three. It is difficult differentiate the mass loss of the

graphite from the silicon. The amount of silica fume in the filter was also measured directly and is presented in Figure 22.

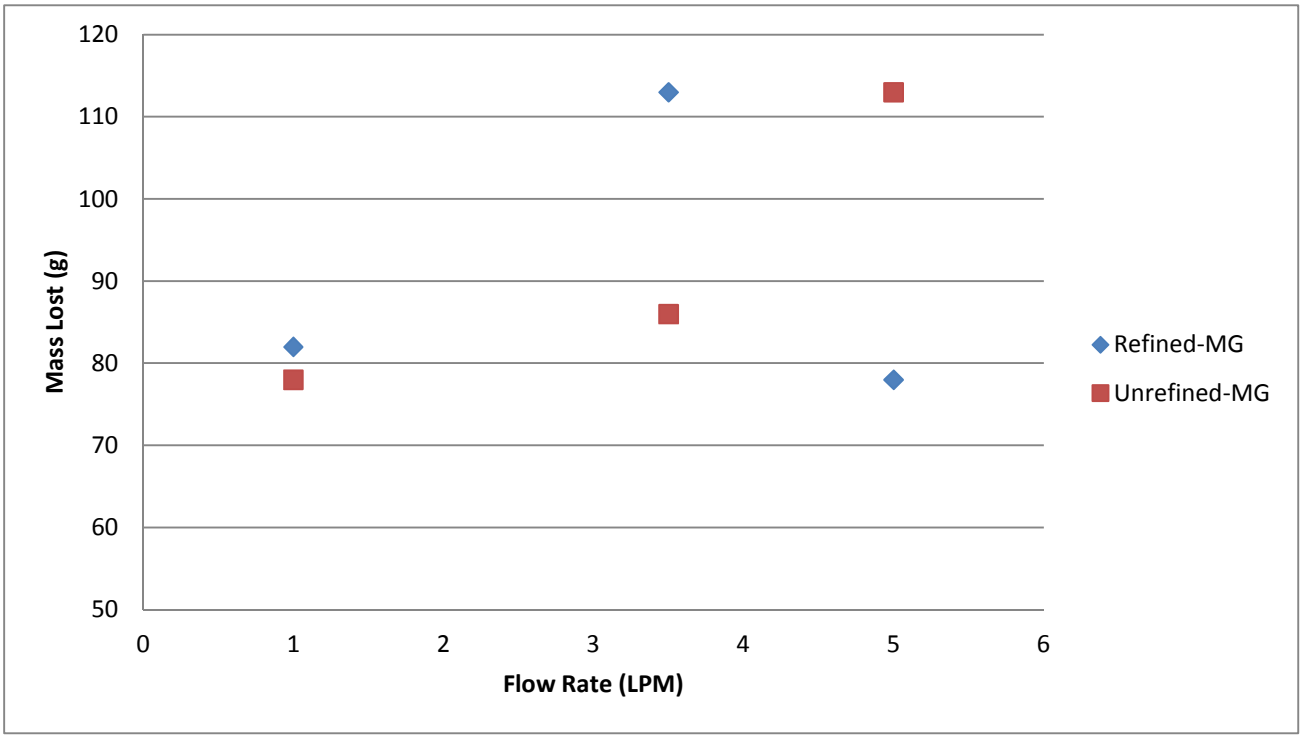

Figure 21--Mass loss from crucible, thermowell and silicon as SiO_2 fume and CO gas.

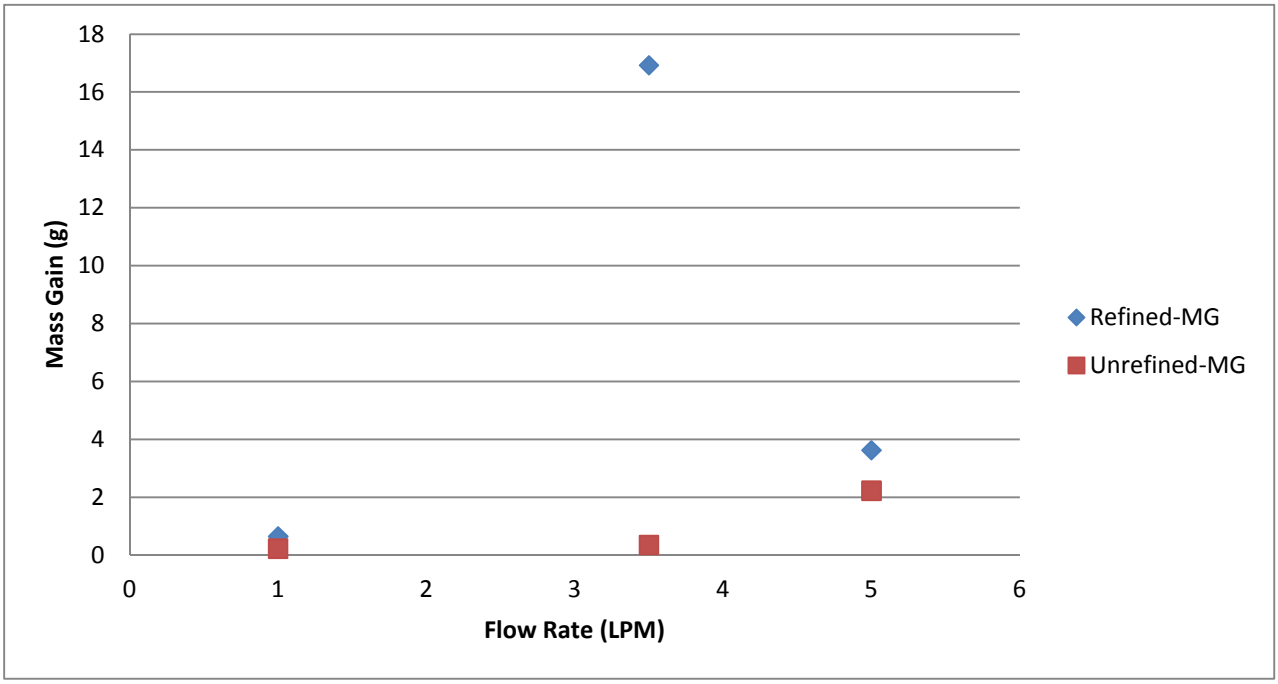

Figure 22--Mass gain of the filter from silica fume.

A significant amount of silica fume accumulated in the tube going from the crucible to the filter this silica had to be taken into account to get an accurate silica flux. The before and after mass was taken, but due to the low density of the silica fume the buildup was not accurately recorded on the scale used. In the experiments with 5 LPM flow rate the large amount of fume allowed for a more accurate weighing. For the experiments at lower flow rates the weight of silica fume had to be estimated from the volume and density of the dust. To estimate the amount of silica fume the amount of build up was measured from photos taken after each experiment. This was used to calculate the mass of silicon in the cooling tube. Since the cooling tube represented only a portion of the silica that was captured before reaching the filter this value was multiplied by 2.5 to get the total amount of fume that was captured in the tubing. The 2.5 scaling factor was determined by carrying out these calculations on the 5 LPM experiments since the final weight was know the appropriate factor could be determined. Figure 23 shows the photos of the three cooling tubes from the experiments with unrefined MG-silicon which were used to measure the amount of silica fume. The estimated silica fume mass in addition to the filter mass were used to estimate the silica flux in moles/s m^2, and the results are presented below in table 5. The silica flux for refined MG-silicon with a flow rate of 3.5 LPM is much higher than the others it is believed that during the course of the oxidation experiment something went wrong and resulted in a much higher flux then is reasonable. This value will be ignored in future discussions.

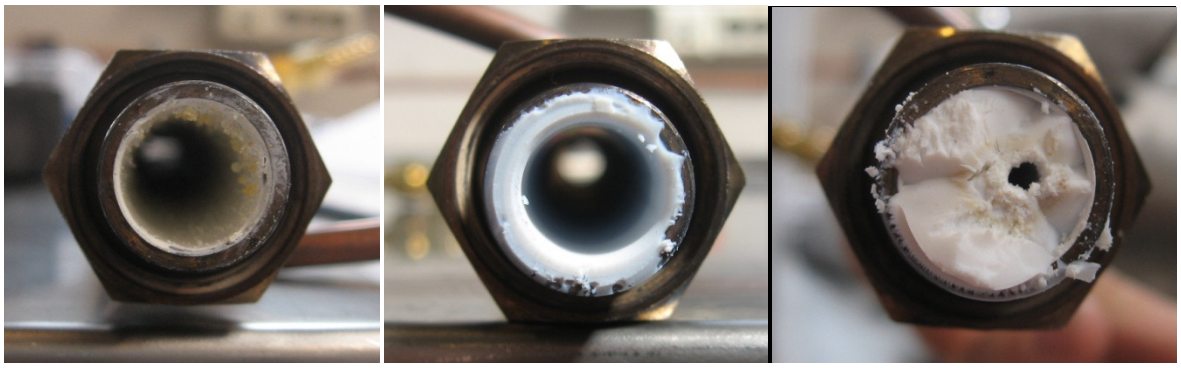

Figure 23--Cooling tubes showing silica dust build up for the 1LPM, 3.5 LPM and 5 LPM unrefined MG-Silicon respectively.

Table 5 Silica flux [moles/s m^2] from weighed and estimated silica dust amounts.

	Refined MG	Unrefined MG
1 LPM	0.00498	0.00156
3.5 LPM	0.12965	0.00276
5 LPM	0.02788	0.01896

4.2.2 SEM Analysis

The morphology of the silica fume was found to be the typical spherical shape that has been well documented. Figure 24 shows an example of the silica dust. Variations in the particle size and composition with air flow rate were found.

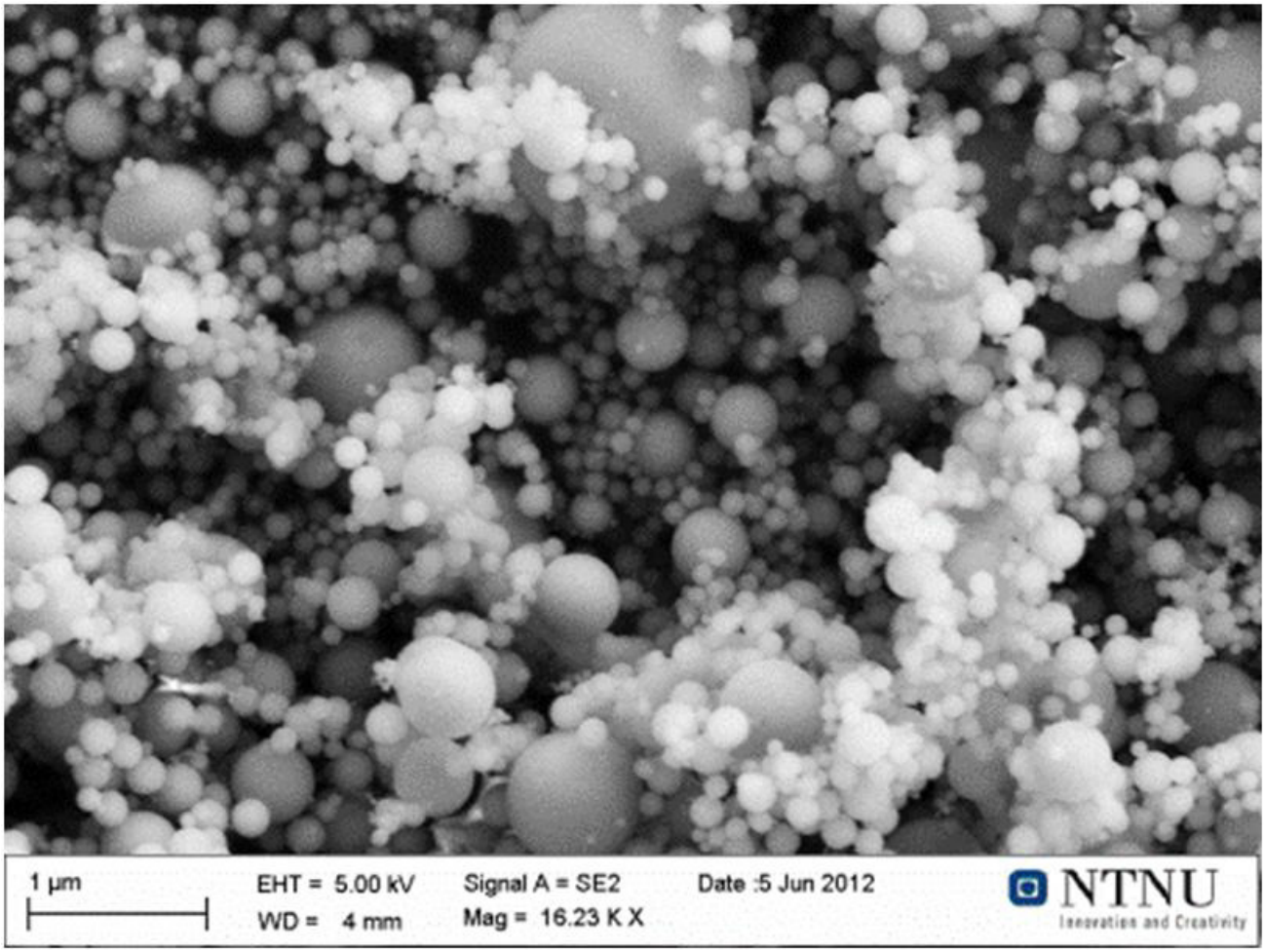

Figure 24--Typical silica fume particle morphology.

Figures 25 and 26 shows the estimated particle size distribution of particles for refined and unrefined MG-silicon. Most particles were below 0.099 µm in diameter and all others were under 1.5 µm with the exception one the large particle which was 3.58 µm. The particle size distribution was seen to change with flow rate. As the flow rate was increased the size and number of large particles decreases. Additionally, unrefined silicon appears to have a higher percentage of large particles at low flow rates than unrefined though this trend is not clear. It should be noted that this is not a true particle size distribution as all the particles were not systematically counted, but the main result is that the number of large particles decreases as flow rate increases. In reality over 75% of the particles are below 0.099 µm in size. SEM images from different flow rates with the unrefined MG-silicon are shown in Figures 27-29. It can clearly be seen from these images that the particle size distribution changes with flow rate.

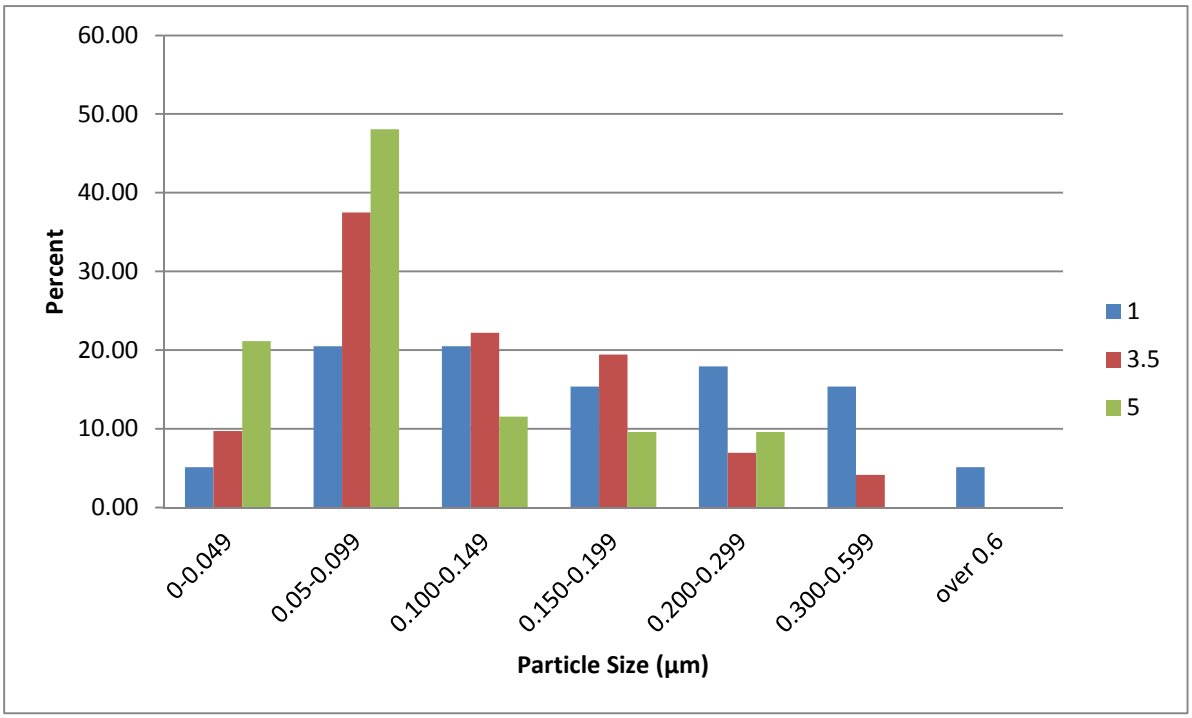

Figure 25--Particle size distribution for refined MG-silicon.

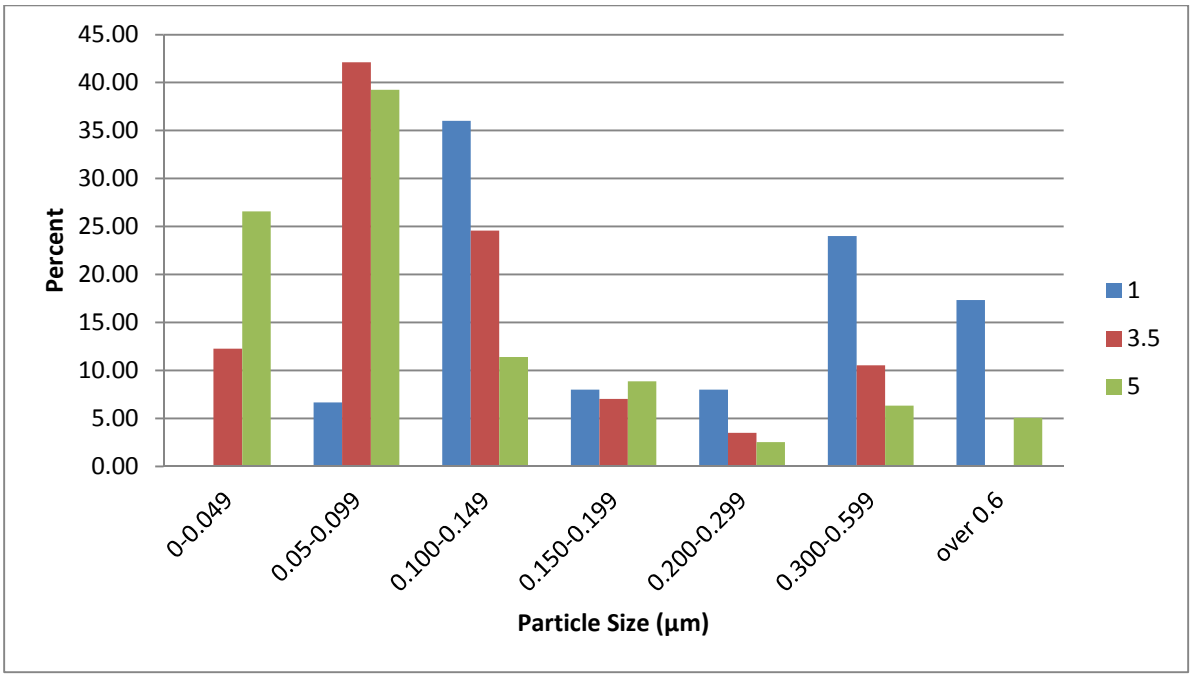

Figure 26--Particle size distribution for unrefined MG-silicon.

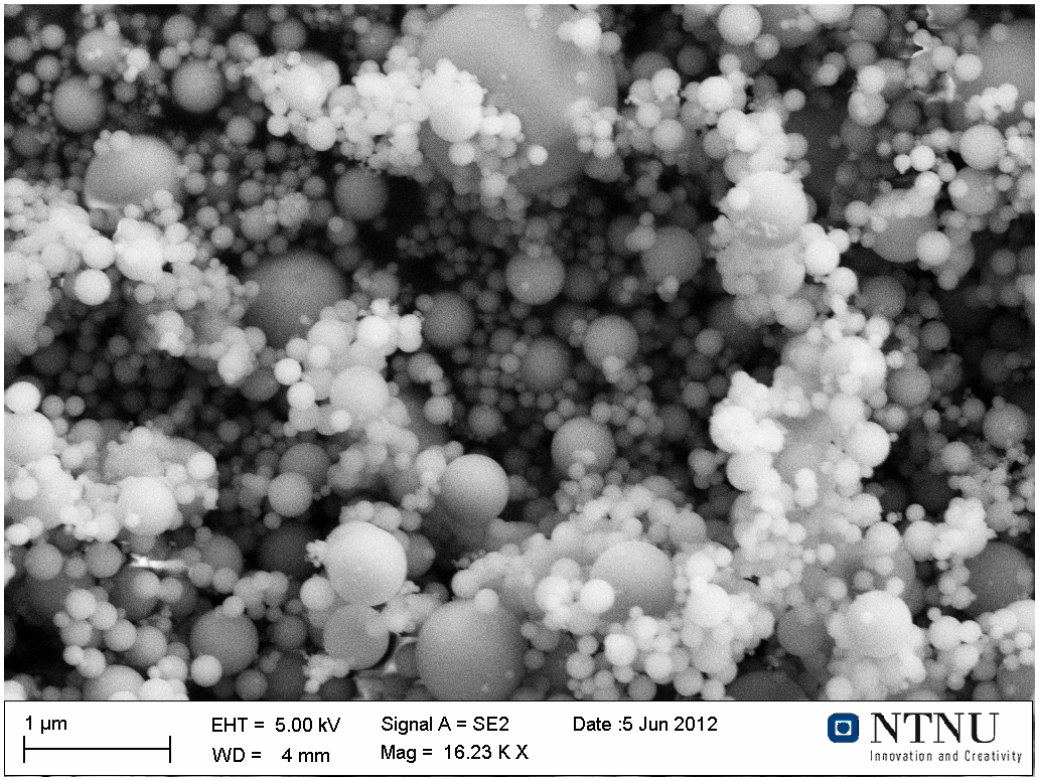

Figure 27-Silica fume from 1 LPM unrefined MG-silicon.

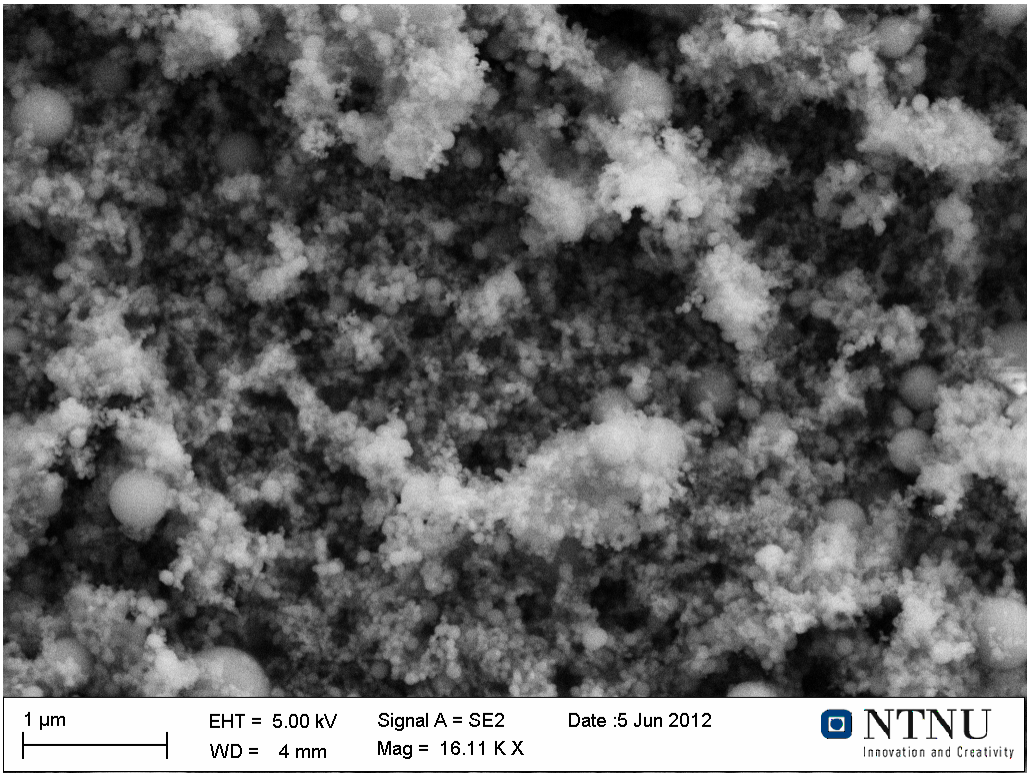

Figure 28--Silica fume from 3.5 LPM unrefined MG-silicon.

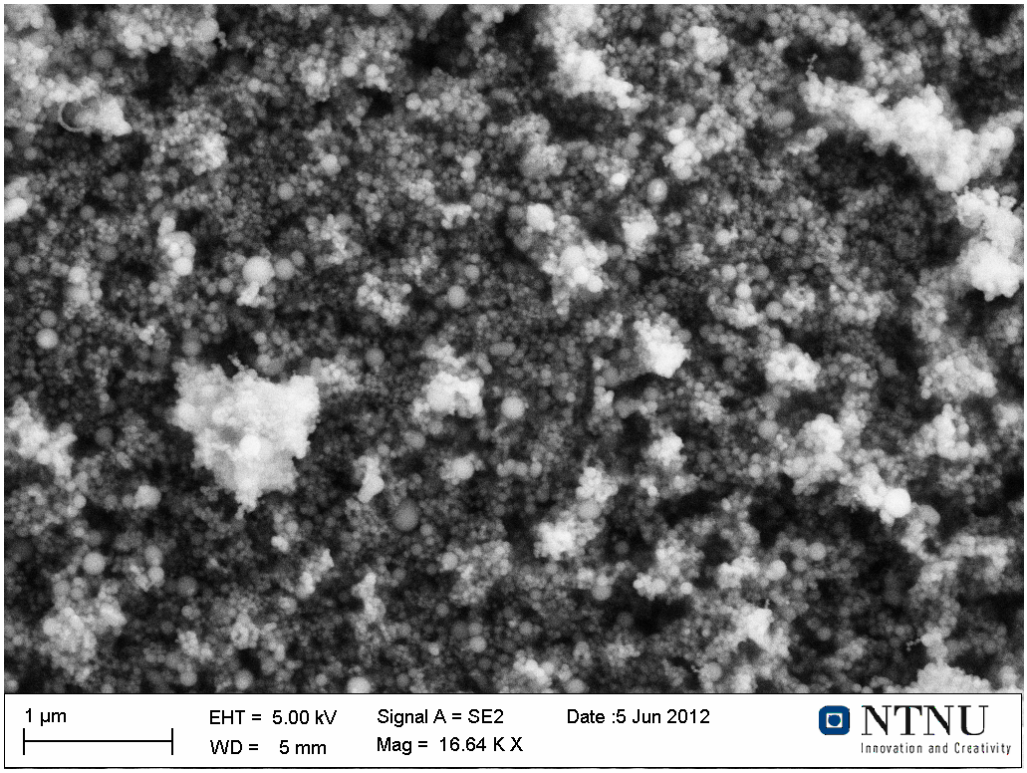

Figure 29-- Silica fume from 5 LPM unrefined MG-silicon.

The composition of the silica fume was examined by EDS. Due to the small particle size it was difficult to analyze individual particles rather groups of particles were examined. Additionally, several of the large particles were examined when ones with a diameter over 1 µm were found. The results from the refined-MG silicon were typical of silica fume. It was found to be primarily SiO_2 with 4.85% CaO at 1 LPM. The unrefined silicon also contained between 9.3-24.3 percent CaO and 0-8.2 percent Al_2O_3. Copper and zinc were also found in a majority of the samples with varying percentages following no apparent trend. Table 6 shows the average composition from the different experiments. The larger particles, that were analyzed individually, were appeared to have calcium and aluminum percentages higher than the groups of small particles. Additionally, several other elements were found at one or two of the analysis points, but never in any significant quantity. These include sodium, potassium, fluorine and magnesium.

Table 6 Average composition of silica fume from each experiment.

	Refined-MG				Unrefined-MG		
	1 LPM	3.5 LPM	5 LPM		1 LPM	3.5 LPM	5 LPM
SiO_2	90.11	96.78	95.41		65.95	87.21	91.81
CaO	4.85	0.00	0.00		24.30	19.84*	9.29**
Al_2O_3	0.00	0.00	0.00		8.22	0.00	0.00
Cu	5.03	1.42	3.06		1.47	4.65	1.95
ZnO	0.00	1.83*	3.45*		0.00	0.00	0.00

* Represents element was found only once at the specific flow rate
**Represents element was found only twice at the specific flow rate

In addition to the changes in particle size distribution the composition of the particles in the experiments with unrefined-MG silicon was found to be affected by flow rate. The change in composition was seen with EDS scans in addition to a distinct color difference between samples when looked at with the naked eye. By referring to Table 6 it can be seen that the CaO and Al_2O_3 amounts decrease with increasing flow rates. Additionally, Figure 30 shows images of the fume collected in the cooling tube from the 3.5 and 5 LPM unrefined MG-silicon experiments, it can clearly be seen that there is a

difference in color between the two flow rates another strong indication of differences in composition.

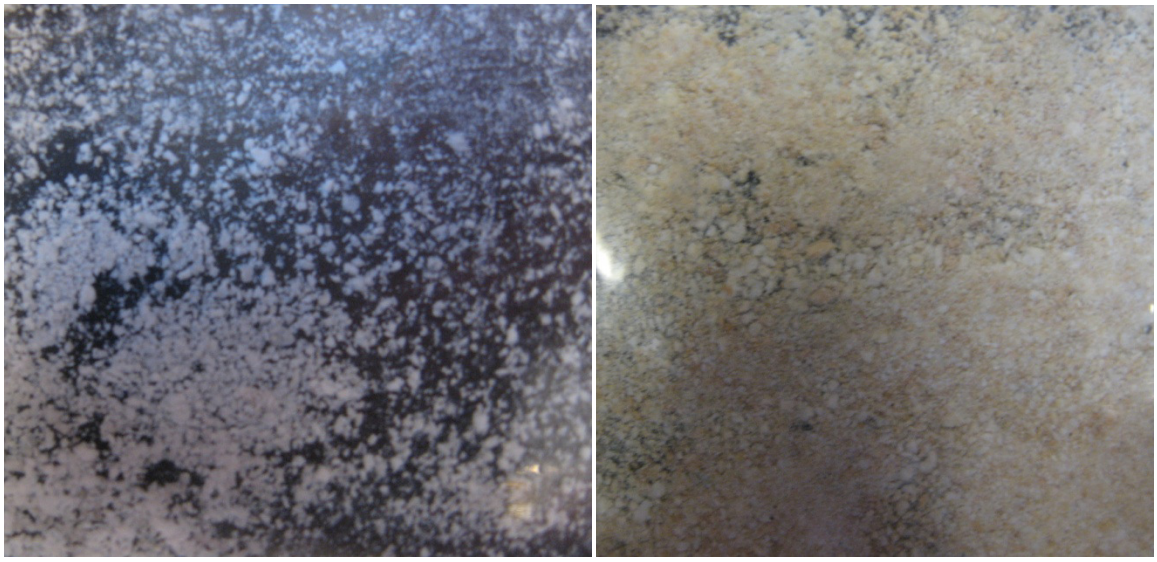

Figure 30-Silica dust collected in cooling tube with 3.5 LPM on the left and 5 LPM on the right

In addition to the typical spherical shape a number of small fibers with a diameter of 10-50 nm were found and are shown in Figure 31. These small fibers were found in all experiments. Typically they formed in or close to the crucible near to the opening for the exhaust gas and on the outside surface of the lance; they were also found inside the filter. Examination of the filter dust found no individual fibers, but rather clusters visible to the naked eye even though individual fibers are too small to be seen by the eye. Figure 32 shows an image of a cluster of fibers without magnification that were built up on the lance. The fiber clusters trapped in the filter were balls less than 0.5 cm in diameter. Due to the fibers small size the composition could not be analyzed by EDS. However, when in the SEM they have a white color very similar to the silica spheres meaning they are primarily silica based.

Figure 31--Small fibers found in all experiments.

Figure 32--Unmagnified image fibers on the lance.

4.2.3 Mass Balance

By using the total fume amounts and the composition data the total amount of the impurity element in fume can be calculated and is presented in Table 7. Even though the percentage in the fume was high the percentage of calcium and aluminum that reported to the fume was small.

Table 7 Percent of impurity element that reported to the fume.

	1 LPM	3.5 LPM	5 LPM
Si	0.004	0.010	0.075
Ca	0.489	0.705	2.267
Al	0.061	0.000	0.000

4.2.4 Graphite Loss to CO Gas

Given the high mass loss from the crucible, silicon and thermowell compared to the amount of silica fume found it the filter it is reasonable to conclude that the bulk of the loss in mass from the crucible is due to the formation of CO gas. Table 8 shows the graphite loss from the crucible. The silicon mass loss was calculated using the silica flux from Table 5. The graphite loss was then calculated by subtracting the mass loss silicon from the mass loss from crucible. Additionally, the mass change of the lid and lance are included. The mass change of the lid is correlated to the number of times it was used. The mass loss increased each time the lid was used. Otherwise no trend exists in the consumption of graphite.

Table 8 Mass loss of graphite from the crucible.

	Refined MG-Silicon				Unrefined MG-Silicon		
	1 LPM	3.5 LPM	5 LPM		1 LPM	3.5 LPM	5 LPM
Mass Loss from Crucible	82.0000	113.0000	78.0000		78.0000	86.0000	113.0000
Mass loss silicon	0.5033	13.1083	2.8186		0.1580	0.2787	1.9165
Mass loss due to graphite	81.4967	99.8917	75.1814		77.8420	85.7213	111.0835
Mass loss of lid	55	54	61		65	55	42
Mass loss of lance	6	22	14		2	9	11

5 Discussion

The results from both experiments raise several questions and require further discussion. The key points that need to be covered are:

- The effect of flow rate on silica flux
- Effect of flow rate on size and composition
- Comparison of refined to unrefined MG-silicon
- Comparison to industrial measurements
- Muffle furnace results
- Comparison of induction furnace and muffle furnace results
- Sources of error

Each of these points will be covered in detail below to give a better understanding of their meaning and answer possible questions.

5.1 Effect of Flow Rate on Silica Flux

The increase of oxidation rate due to increasing flow rate is due to several reasons. The main reason is probably that the supply of oxygen to the surface has been increased. While the partial pressure of oxygen remained unchanged in all the experiments the quantity of oxygen supplied to the surface is increased. Since oxygen will react instantaneously when interacting with Si and SiO an increase in the oxygen flux will result in an increase of the silicon flux.

Additionally, when the flow rate is increased the velocity also increases this results in the diffusion boundary layer thickness being reduced. However, probably due to turbulence of the system the oxide does not form on the surface and remains in the active oxidation regime. Even though the models discussed in the theory would predict the surface to be passivated when the oxygen partial pressure 0.21 atm. This reduced boundary layer reduces the time it takes for the gaseous diffusion resulting in an increased silica flux.

Finally, with an increased flow rate and gas velocity the surface of the silicon bath will become more turbulent, thus increasing the apparent surface area. However, this effect is small compared to the increased mass flow of oxygen to the system and decreased boundary layer thickness.

5.2 Effect of Flow Rate on Size and Composition

The difference in size distribution can be explained by looking at the time a particle has to oxidize. Oxidation and growth can only occur in the presence of SiO and high temperatures the region that these conditions exist is limited. Once the particle has left this region it cannot oxidize and grow larger. Therefore, in order for a silica particle to grow larger the time in the SiO rich environment must be increased, which occurs at lower flow rates. In other words, at higher flow rates a silica particle leaves the crucible a much shorter time after nucleation than it does at low flow rates thus resulting in smaller sized particles.

With respect to unrefined MG-silicon the reasons for the reduced CaO and Al_2O_3 amounts at higher flow rates could be that with the high flow rates there was not enough time for the silica to react with calcium and aluminum to form to CaO and Al_2O_3 as discussed in the theory section. The probability of this interaction happening are much higher the longer the silica particle remains in the vicinity of the silicon melt which occurs at lower flow rates. This also helps to explain why the larger particles often had a higher CaO and Al_2O_3 content then the smaller particles.

In Table 7 it can be seen that the percentages of calcium and aluminum reporting to the fume is low. This is in good agreement with the industrial measurements which found that calcium and aluminum would report to the fume, but in much smaller percentage then to the slag or metal. In the case of this work where no slag for the CaO and Al_2O_3 couldn't report to the metal likely retained a higher level of the impurities. This is likely due to the fact that under active oxidation it is difficult for the calcium and aluminum to leave the silica melt due to the low vapor pressure compared to SiO.

5.3 Comparison of Refined to Unrefined MG-Silicon

Several differences between refined and unrefined MG-silicon have been noted. These include oxidation rate, silica dust composition and size distribution differences. There appears to be a difference in flux between refined and unrefined MG-silicon. This difference is small and given the accuracy of the measurements no conclusions can be drawn from it. The differences in composition are simply because the aluminum and calcium content of melt are higher creating a higher concentration of the impurities in the silica dust.

5.4 Comparison to Industrial Measurements

Industrial measurements of the silica fuming rate were undertaken by Mari Næss as part of the Fume project and were presented in the theory section. Næss found the flux to vary from 0.031-0.079 Moles/s-m^2 opposed to the 0.00156 to 0.02788 moles/s-m^2 for this work (refer to Tables 3 and 5). It can be seen that the silica flux found for these experiments is one order of magnitude lower at low flow rates and on the same order at higher flow rates. The primary reason for the lower silicon flux is the difference in flow rates in the industrial measurements the gas purge rate varied from 50-283 LPM which is higher than the 1-5 LPM used in this work. Taking into account the lower gas flow rate the lower silicon fluxes are agreeable to the industrial measurements and can be a good indication as to how industrial processes may perform. In addition the particle sizes were found to be in the similar size range. Overall the experiments in the medium scale induction furnace are comparable to the industrial measurements, as the reaction mechanism and product are similar, and the silicon fluxes are comparable.

5.5 Muffle Furnace Experiments

The results from the experiments and EPMA analysis are similar to what was found in previous work. The formation of small spherical drops of silicon would indicate that they nucleated inside the oxide layer possibly during cooling as the SiO gas condensed.

The primary reason for the high CaO and Al_2O_3 formation primarily occurring at the oxide metal interface can be explained by the typical reaction mechanism used for slag refining of silicon. Where due to its high activity the oxygen first reacts with silicon to form SiO_2 then in the presence of aluminum or calcium the oxide will react to form CaO

or Al_2O_3 and Si. The SiO_2 oxide layer formed first then based on the diffusion of aluminum and calcium to the oxide-metal interface it is consumed to give CaO and Al_2O_3. Additionally, within the oxide layer the two oxide phases reacted with each other. This resulted in the two phases becoming more homogenous in content and a the rounding of the phase boundaries as seen in Figures 18 and 19.

5.6 Comparison of Induction and Muffle Furnace Experiments

Several differences exist between the results from the experiments carried out in the muffle furnace and those done in the induction furnace. The differences can be explained by recalling the differences between active and passive oxidation. The muffle furnace experiments fell under the passive oxidation regime, whereas, the induction furnace experiments resulted in active oxidation of the silicon. The largest difference was the effect that the aluminum and calcium had on the oxidation. In the muffle furnace experiments aluminum was the major element found in the oxide product where as the induction furnace experiments found calcium to be more prevalent. The higher vapor pressure of the calcium then aluminum resulted in high losses when the oxidation occurred in the gas phase (active oxidation) above the melt surface, whereas when the reaction was occurring on the melt surface the higher affinity of aluminum for oxygen played a bigger role.

5.7 Sources of Error

There were several sources of error within the induction furnace experiments. The sources of error for the muffle furnace experiments were given in the project report and will not be repeated here. Below is a list of errors for the induction furnace experiments.

- Loss of graphite materials as CO gas
- Mass measurements inaccuracies
- Instability of the system.

The largest loss of mass from the crucibles was due to the formation of CO gas and not silica fume. This makes calculation of the silicon mass loss difficult. It would be best to eliminate or reduce the loss to CO gas. This could be done through several methods.

First, since the primary graphite loss occurs on the outside of the crucible it could be coated with a non-permeable material like boron nitride or Al_2O_3. Since only the outside of the crucible would need to be coated no reactions with the silicon and coating would occur and the silicon flux could be measured in a more direct and accurate manner. Second, a baseline run could be carried out where a crucible with no silicon was placed in the furnace and held at 1550℃ for 20 minutes then the measured mass loss could be subtracted from the results of the oxidation experiments.

The second source of error was due to the balance used to measure the mass before and after oxidation was not precise enough to give the mass gain in the tubing going from the crucible to the filter. A balance with an accuracy of 0.05 grams that can handle loads up to 1500 grams should have been employed.

Finally, the oxidation system itself was not completely identical every time. For example the experiment at 3.5 LPM and refined MG-silicon showed a high mass change. This was likely due to some variable not being kept the same. Since all variables must be kept by hand it is difficult to look back and see where any discrepancies may have occurred; if the temperature and air flow could be logged on a more continuous manner it would provide more information into how the system preformed. Additionally, in the last experiments the thermocouple began to fail and its accuracy could not be ensured. Meaning the temperature possibly had a large variance, but given the limited impact of temperature in between the 1450-1650℃ range this was a minor issue. Lastly, it was difficult to run each experiment in exactly the same procedure. For example in the experiment at 5 LPM with unrefined MG-silicon when the lance was being removed at the end of oxidation the lance stuck and the lid came off exposing the silicon to open air. The effect this had on the results is unknown; it did result in some of the silica fume not being captured while the system cooled down.

6 Conclusion

A series of experiments were carried out to examine the effect of air flow rate on the silica flux in a medium scale induction furnace. In addition to changes in the silica flux fume samples were also collected and analyzed in by SEM and EDS. The experiments were modeled after the industrial refining of silicon were aluminum and calcium are the major impurities. Therefore, refined and unrefined MG-silicon were tested at 3 different flow rates of 1, 3.5 and 5 LPM. The silicon surface remained bare in the experiments and was under an active oxidation regime for all the experiments. the following results were found.

- The silica flux was found to increase with increasing flow rate from 0.00498 and 0.02788 moles/s-m^2 for refined and from 0.00156 and 0.01896 moles/s-m^2 for unrefined.
- Particle size analysis found the typical spheres shape with the same size distribution as found in industrial silica fume with more than 75% of the particles being smaller than 0.1 µm in diameter and with a max diameter of 1.5 µm.
- Particle size was found to vary with air flow rate. The size and frequency of the large particles was found to decrease with increases in flow rate.
- With respects to the unrefined MG-silicon a change in composition with flow rate was found. At 1 LPM the fume had a CaO was found at all analysis points with an average of 24.3% at 5 LPM CaO was found at only 2 points with an average of 9.29%. The Al_2O_3 content was found to decrease from 8.22% to 0% going from 1 to 5 LPM. A mass balance of the impurity elements found that less than 3% of them had reported to the fume which is consistent with industrial observations.
- In comparison to industrial measurements the results are in good agreement. Showing silica fluxes on the same order of magnitude or one order lower. Which considering how the flow rates in the medium scale experiments were lower than industry it is considered to be in good agreement. Additionally, the reaction mechanism and product is similar.

- The continuation of work done in the muffle furnace showed that under the passive oxidation regime the addition of calcium has the largest affect on oxidation rate.

- The oxide layer that forms on samples containing both aluminum and calcium were complex and contained multiple phases: one high in Al_2O_3 and one primarily composed of SiO_2. These to phases reacted with time and the phase boundaries softened and the composition difference was lessened.

This work has shown that the air flow rate over the silicon melt has a significant effect on the oxidation and fuming rate of the liquid silicon. Furthermore it was shown that the medium scale induction furnace can produce results in good agreement with industrial measurements and therefore can be used to simulate fuming industrial silicon production.

7 Future Work

Continuation of the medium scale induction furnace experiments is planned. Since it has been shown that the system can be used to approximated industrial refining ladles. More experiments will be carried out to test a larger range of flow rates, gas composition, metal composition. Additionally, steps should be taken to eliminate the problem of graphite loss to CO gas. Further analysis of the fume by SEM, EDS, EPMA and ICP-MS should be done to confirm the results and attempt to explain the formation of the silica fibers. Finally several of the experiments will be repeated to check for reproducibility.

8 References

1. *Passivity during the Oxidation of Silicon at Elevated Temperatures.* **Wagner, Carl.** 9, s.l. : Journal of Applied Physics, September 1958, Vol. 29.

2. *Enhancment of Diffusion-Limited Rates of Vaporization of Metals.* **Turkdogan E.T., Grieveson P., Darken L.S.** August 1963, Vol. 67.

3. *The High Temperature Oxidation, Reduction, and Volatilization Reactions of SIlicon and Silicon Carbide.* **Gulbransen, E. og Jansson, S.** 3, s.l. : Oxidation of Metals, 1972, Vol. 4.

4. *The Active Oxidation of Si and SiC.* **Hinze, J.W. og Graham, H.C.** 7, s.l. : Journal of the Electrochemical Society, July 1976, Vol. 123, ss. 1066-1073.

5. **Schei, A., Tuset, J og Tveit, H.** *Production of High Silicon Alloys.* s.l. : Tapir, 1998.

6. **Gaskell, D.R.** *Introduction to the Thermodynamics of Materials.* s.l. : Taylor and Francis, 2003.

7. *Mechanisms and Kinetics of Liquid Silicon Oxidation During industrial Refining.* **Næss, M., et al.** s.l. : Oxid Met, 2012.

8. *Material Balances of Trace Elements in the Ferrosilicon and Silicon Processes.* **Myrhaug, E. og Tveit, H.** Orlando, Florida : s.n., 2000. 58th Electrical Furnace Conference.

9. *Element Distribution in Silicon Production and Refining-Part 1: Mass Flows through the Refining Ladle.* **Næss, M., et al.** 2012.

10. **Smith, N.** *Oxidation Kinetics and Mechanisms of Silicon and Si-Al-Ca Alloys.* 2011. Project Report for TMT5500.

11. **Lapointe, Kyle.** *Oxidation of Silicon Progress Report.* 2011.